

Quantum Langevin Dynamics for Optimization

Zherui Chen* and Yuchen Lu*

Xingjian College, Tsinghua University, Beijing 100084, China

Hao Wang

School of Electronics Engineering and Computer Science, Peking University, Beijing 100871, China

Yizhou Liu[†]

Department of Engineering Mechanics, Tsinghua University, Beijing 100084, China

Tongyang Li[‡]

Center on Frontiers of Computing Studies, School of Computer Science, Peking University, Beijing 100871, China

(Dated: November 28, 2023)

We initiate the study of utilizing Quantum Langevin Dynamics (QLD) to solve optimization problems, particularly those non-convex objective functions that present substantial obstacles for traditional gradient descent algorithms. Specifically, we examine the dynamics of a system coupled with an infinite heat bath. This interaction induces both random quantum noise and a deterministic damping effect to the system, which nudge the system towards a steady state that hovers near the global minimum of objective functions. We theoretically prove the convergence of QLD in convex landscapes, demonstrating that the average energy of the system can approach zero in the low temperature limit with an exponential decay rate correlated with the evolution time. Numerically, we first show the energy dissipation capability of QLD by retracing its origins to spontaneous emission. Furthermore, we conduct detailed discussion of the impact of each parameter. Finally, based on the observations when comparing QLD with classical Fokker-Plank-Smoluchowski equation, we propose a time-dependent QLD by making temperature and \hbar time-dependent parameters, which can be theoretically proven to converge better than the time-independent case and also outperforms a series of state-of-the-art quantum and classical optimization algorithms in many non-convex landscapes.

I. INTRODUCTION

Continuous optimization is a branch of optimization theory concerned with the optimization of continuous variables within a mathematical model. Within this domain, gradient descent and its improved versions emerge as a widely embraced subclass of continuous optimization algorithms, having achieved widespread utilization across diverse domains, including but not limited to machine learning and associated disciplines [1–4]. More recently, there have been systematic studies of gradient descents via the analysis of their continuous-time limits as differential equations [5–8]. In particular, the continuous-time limit of stochastic gradient descents become the overdamped Langevin equation [9], and algorithms based on the classical Langevin equation with stochastic gradients were previously proposed and widely used in various machine learning and Bayesian modeling contexts [10–12], such as the Stochastic Gradient Langevin Dynamics algorithm for nonconvex optimization [13], Langevin Monte Carlo for sampling [14], continuous-time Langevin diffusion for stochastic calculus [15], etc. Over the preceding decades, efficient quantum algorithms for various optimization problems have been proposed, including linear

programming [16–20], semi-definite programming [21–26], polynomial optimization [27, 28], convex optimization [29, 30], escaping from saddle points for nonconvex optimization [31], etc. Despite this, leveraging the nature of quantum mechanics to propose powerful optimization algorithms [31–33] is still a challenging task and solicits further developments.

The Bregman-Lagrangian framework was proposed in Ref. [6], which generated a large class of accelerated methods in the continuous-time limit. Ref. [32] derived Quantum Hamiltonian Descent (QHD) by using the propagator of the quantum dynamics to quantize the Bregman-Lagrangian framework. When taking stochastic noise into account, Ref. [9] provided a general theoretical analysis of the effect of the learning rate in Stochastic Gradient Descent (SGD). Viewing SGD from the perspective of dynamic systems, it can be considered as a specific classical open dissipative system with stochastic noise, named as classical Langevin system [9, 34, 35]. This observation inspired us to harness a distinct category of open dissipative quantum systems, known as quantum Langevin system [36], with the explicit purpose of constructing an optimization algorithm.

Physically, the mutual influence of a system, with a few degrees of freedom, and a heat bath, with many degrees of freedom, on each other is the central concept in the physics of noise both in quantum and classical cases. The variables within the bath exert an influence on the system by introducing stochastic terms into the system's

* These authors contributed equally to this work.

[†] liuyz18@tsinghua.org.cn

[‡] tongyangli@pku.edu.cn

equations of motion. Langevin introduced a class of equations to describe this kinds of classical systems:

$$m\ddot{x} = -\nabla V(x) - \gamma\dot{x} + \sqrt{2\gamma kT}\xi(t). \quad (1)$$

The analogous equations for quantum systems have been formulated and have found applications in numerous instances of physical interest [36]. The quantum case under consideration involves a model of a heat bath comprising harmonic oscillators characterized by distinct masses m_n and spring constants k_n . The Hamiltonian governing the entire system is expressed as follows [36, 37]:

$$H_{total} = H + H_B \\ = H + \sum_n \left(\frac{p_n^2}{2m_n} + \frac{k_n}{2}(q_n - X)^2 \right), \quad (2)$$

where $H = p^2/(2m) + V$ is the Hamiltonian of the system and X represents a specific operator within the system that is coupled with the heat bath. Here, p is the momentum operator of the system, m is the mass of the system, V represents the potential energy of the system, q_n and p_n are the position and momentum operator of the n -th oscillator, respectively.

In order to exploit quantum Langevin dynamics for solving optimization problems, we need a suitable framework for describing quantum Langevin systems. The quantum Langevin equation for an arbitrary system operator Y can be readily derived from the Heisenberg equation of motion [38], i.e.,

$$\dot{Y} = \frac{i}{\hbar} [H_{total}, Y]. \quad (3)$$

However, we are manipulating operators in quantum mechanics, which makes the analysis of above equation of motion highly challenging. Therefore, we adopt the Born-Markov approximation and use path integral approach [39, 40] to solve this challenge. When the correlation time of the noise is significantly shorter than the typical time scale of the damped motion of the system, we obtain the quantum Brownian motion master equation [36, 39, 40]:

$$\frac{d\rho}{dt} = -\frac{i}{\hbar} [H, \rho] - \frac{\eta}{\hbar} \left(\frac{2mkT}{\hbar} [x, [x, \rho]] + i[x, [p, \rho]]_+ \right) \quad (4)$$

where $H = p^2/(2m) + V$, p is the momentum operator of the system, x is the position operator, and $\eta = \gamma/2m$ represents the characteristic damping rate with system mass m , k is the Boltzmann constant. However, it is well known that this master equation is only applicable in high-temperature scenarios and fails to satisfy the positivity constraint of the density operator [41–43]. Ultimately, we refer to Ref. [41] and employ Lindblad functional (Eq. (15)) to describe the quantum Langevin dynamics, with a detailed introduction provided in Section II B.

The **optimization problem** we consider is to find the global minimum of a (convex or nonconvex) function $V(x)$:

$$\min_x V(x), \quad (5)$$

where $V(x)$ is assumed to be continuously differentiable in the domain and is also the potential energy of the system in Eq. (15). One can implement Quantum Langevin Dynamics (QLD) by starting from an easily prepared initial state and evolving the quantum system according to Eq. (15). The global minimum of the objective function $V(x)$ can be obtained by measuring the position observable x at the end of the evolution. Therefore, our objective is to establish a theoretical foundation guaranteeing the convergence to the global minimum of QLD. When the parameters of QLD is time-independent, namely, η , \hbar and T are constants during evolution, we establish the convergence of QLD within convex landscapes and specific instances of slightly nonconvex scenarios. Informally speaking, with approximation of $\hbar\Omega \ll kT$ where Ω is the oscillator frequency of the ground state near the global minimum, we have the convergence rate of the average potential,

$$\langle V \rangle_t - V(x^*) \leq 2kf(T) + O(e^{-\eta t}), \quad (6)$$

where $\langle V \rangle_t$ denotes the expectation value of V with respect to the density matrix of the system, $V(x^*)$ is the potential value at the global minimum x^* and $f(T)$ is a function with respect to T that satisfies $\lim_{T \rightarrow 0} f(T) = 0$. Consequently, the average energy of the system can approach zero in the low temperature limit. When V is a quadratic form, the evolution of the system has an analytical solution. One interesting discovery related to the quadratic potential is that the system can reach the ground state of the quadratic potential when the evolution time $t \rightarrow +\infty$ and $T \rightarrow 0$. Formal description can be found in Section III. However, it is always challenging to give a convergence in the general nonconvex case. Despite our best efforts, we are constrained to confine our theoretical discussions to slightly nonconvex cases. Thus, for other nonconvex landscapes, we resort to meticulous numerical experiments to compensate for the absence of theoretical assurances.

In the realm of numerical experiments, we initially substantiate our intuition regarding the fundamental cause of energy dissipation in QLD. Noteworthy is the observation that despite the finite nature of the heat bath, the system retains the capacity to escape local minima, transitioning from excited states to ground states due to spontaneous emission. In alignment with our theoretical findings, we execute experiments within quadratic frameworks, drawing comparisons with analytic solutions to demonstrate a high degree of concordance. To offer optimal strategies for harnessing thermal and tunneling effects when confronting intricate nonconvex problems, we engage in a detailed discussion delineating the role of each parameter. Broadly speaking, our results indicate

that η determines the convergence rate, temperature T reflects the thermal effect to some extent and \hbar reflects the tunneling effect.

We conduct a comparative analysis between time-independent QLD and overdamped classical Langevin dynamics. In the majority of landscapes that classical dynamics can adeptly resolve, time-independent QLD does not demonstrate any discernible advantages. However, a notable advantage becomes evident in highly non-convex landscapes. At elevated temperatures, classical dynamics exhibits superior performance by supplying the requisite energy to escape local minima. In contrast, time-independent QLD excels in low-temperature environments. This observation substantiates our intuition that quantum noise differs fundamentally from its classical counterpart, as depicted in Fig. 1. Quantum Hamiltonian Descent (QHD) [32] exclusively leverages the tunneling effect and surpasses a curated selection of state-of-the-art gradient-based classical solvers, as well as the conventional Quantum Adiabatic Algorithm (QAA) [32]. It has been demonstrated that noise confers benefits upon classical algorithms in nonconvex landscapes, whereas its impact on quantum algorithms remains unexplored.

Building upon these observations, we find it imperative to explore the realm of time-dependent QLD. Specifically, we recognize the need for pronounced thermal and tunneling effects initially to facilitate escape from local minima. As the system converges to its final stage, these effects need to be gradually deactivated. Consequently, we present a theoretical analysis for time-dependent QLD and propose a cooling strategy for implementation. The convergence of time-dependent QLD is similar to the time-independent one when $\hbar = \hbar(t)$ decreasing monotonically with respect to time and $\eta = \eta(t)$, which says $\langle V \rangle_t - V(x^*) \leq 2kT + O(e^{-\int_0^t \eta(t') dt'})$. For the case of time-dependent temperature, there exists a cooling strategy $T = T(t)$ that guarantees the convergence. In numerical experiments, time-dependent QLD significantly outperforms its time-independent counterpart and surpasses other algorithms, including QHD, QAA, and SGD, across a diverse array of landscapes. In theory, the query complexity of QLD is $\tilde{O}(t)$, which is also among the top tier of all other algorithms.

The rest of this paper is laid out as follows. In Section II, we introduce our notations and provide details for quantum Langevin equation and explicit description of QLD in Eq. (15). Theoretically, we prove the convergence of QLD in convex case (Theorem 1) and slightly nonconvex case (Theorem 2), refer to Section III. Numerically, we first trace back to spontaneous emission to show the essential cause of energy dissipation in QLD, which verifies our intuition, see Section IV A. Then we verify our theoretical results of quadratic case in Section IV C and discuss the roles of each parameter and their relations with thermal and tunneling effects in Section IV D. In Section V we compare QLD with classical dynamics, which informs the development of time-dependent QLD to fully leverage the advantages inherent in quantum dy-

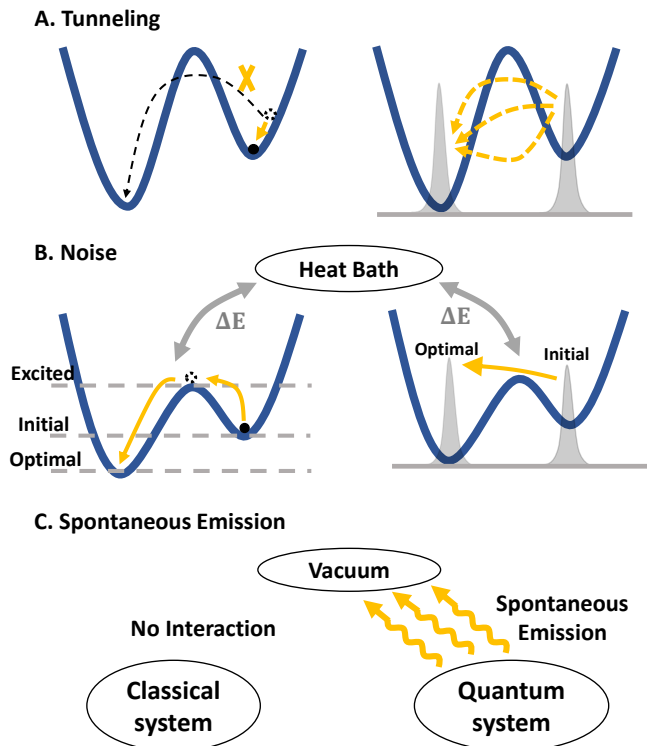


FIG. 1. Differences between classical dynamics (left) and quantum dynamics (right). **A.** Tunneling effect: An illustrative example where classical Gradient Descent algorithms will be trapped because of bad initialization, while quantum algorithms can escape easily. **B.** Noise: The effect of noise can be described by the system coupling with a heat bath. **C.** Special thing of quantum noise: The crucial difference between classical noise and quantum noise emerges when interacting with vacuum. Owing to the principles of quantum mechanics, spontaneous emission exists even in a vacuum heat bath, which indicates the fundamental origin of energy dissipation in the quantum Langevin system.

namics. In Section V A, we prove the convergence of time-dependent QLD in convex case. The performance of time-dependent QLD is evaluated in eight representative landscapes, demonstrating superior performance through comparisons with QHD, QAA, and classical algorithms, shown in Section V F. Finally, we evaluate and compare the query complexity of QLD with other algorithms in Appendix B, demonstrating that QLD is superior to other algorithms in terms of query complexity.

II. PRELIMINARIES

Notations. We denote the Hamiltonian of system as H , the Hamiltonian of heat bath as H_B , the Hamiltonian of heat bath and system as $H_{total} = H + H_B$. Let E_k be the kinetic energy of the system and V be the potential energy of the system, so $H = E_k + V$. Given two quantum operators A and B , we use $[A, B] = AB - BA$ for denoting the commutation, while $[A, B]_+ = AB + BA$

for the anti-commutation. We denote the characteristic damping rate of the system as η and the temperature of heat bath as T . Given a quantum operator $O(t)$, its time-dependent expectation value with respect to density matrix $\rho(t)$ is calculated by $\langle O(t) \rangle_t = \text{Tr}(\rho(t)O(t))$.

A. Quantum Langevin Dynamics (QLD)

In this subsection, we provide a succinct introduction to the genesis of Quantum Langevin Dynamics (QLD) within the Heisenberg picture, and elaborate on our motivation for employing it in optimization tasks. It is well-established that the continuous-time limit of Stochastic Gradient Descent aligns with the classical Langevin equation [9, 44]. Some researches have extended the classical Langevin equation to the quantum case. Ref. [37] put forward the following Hamiltonian for the dynamics of a quantum system coupled to a heat bath:

$$H_{total} = H + \sum_n \left(\frac{p_n^2}{2m_n} + \frac{k_n}{2} (q_n - X)^2 \right), \quad (7)$$

where X is a specific system operator and the heat bath is simplified as a set of harmonic oscillators with different masses m_n and spring constants k_n [36, 37]. This kind of coupling characterizes what happens for electromagnetic radiation, but is not appropriate in some other situations such as electrical resistance in a metal [36].

Originated from Eq. (7), Ref. [45] gave a dynamical description of a system moving in a potential, which can be considered as a quantum version of the classical Langevin equation for the motion of system in a potential under the influence of viscous drag and a fluctuating force [36, 45]. Set the Hamiltonian of one-dimensional system to be $H = \frac{p^2}{2m} + V(x)$, where p is the system momentum operator, m is the mass of the system, x is the system position operator and $V(x)$ is the potential function. Under the Heisenberg picture, we can get the equation of motion for the system from Eq. (7) by setting $X = x$ [36, 45],

$$m\ddot{x}(t) = -V'(x(t)) - \int_0^t f(t-t')\dot{x}(t')dt' - f(t-0)x(0) + \xi(t), \quad (8)$$

where $f(t)$ is the memory function, which makes the equation of motion at time t be influenced by the values of $\dot{x}(t)$ at preceding moments, and $\xi(t)$ is the noise term, with forms

$$f(t) = \sum_n k_n \cos \omega_n t, \quad (9)$$

$$\xi(t) = \sum_n \left(q_n(0)k_n \cos \omega_n t + \dot{q}_n(0)\sqrt{k_n m_n} \sin \omega_n t \right). \quad (10)$$

Here, $\omega_n = \sqrt{k_n/m_n}$.

Under the first Markov approximation and the continuum-spectrum approximation [36], we obtain

$f(t) = 2\gamma\delta(t)$, where γ is a damping constant and $\delta(t)$ is the Dirac delta function. Then we get the quantum Langevin equation in the Heisenberg picture, which has the same form as the classical Langevin equation [9, 35, 44] in the underdamping limit but is fully quantum mechanical,

$$m\ddot{x}(t) = -V'(x(t)) - \gamma\dot{x}(t) + \xi(t). \quad (11)$$

While dissipation in quantum mechanics is described by quantum Langevin equation to some extent, analyzing the dynamics of this open quantum system remains to be a such challenging task that we can hardly move a step forward with Eq. (11) in the Heisenberg picture when studying the convergence of QLD. In order to solve this challenge, we introduce the Lindblad functional for QLD in the next section.

B. Lindblad functional for QLD

Density matrix approach is often used to describe the dynamics of an open quantum system. Based on this point, Caldeira and Leggett proposed a well known master equation named after themselves as the Caldeira-Leggett equation [36, 40] to describe the dynamics of quantum Langevin system. However, the Caldeira-Leggett equation faces some serious problems, such as the non-positivity of the density matrix and only available for high temperature region [41–43]. Refs. [41, 46] fixed these problems by introducing a Lindblad equation, which is a more general form of the Caldeira-Leggett equation.

A Lindblad equation can be presented in the standard form:

$$\begin{aligned} \frac{d\rho}{dt} &= \mathcal{L}(\rho) \\ &= -\frac{i}{\hbar} [H, \rho] + \sum_{j=1}^m \left(2L_j \rho L_j^\dagger - [L_j^\dagger L_j, \rho]_+ \right). \end{aligned} \quad (12)$$

Ref. [41] studied the case where the Hamiltonian H is given by $H = \frac{p^2}{2m} + V$ and the unique Lindblad operator L is a linear combination of position operator x and momentum operator p ,

$$L = (\mu x + i\nu p), \quad L^\dagger = (\mu x - i\nu p), \quad (13)$$

where

$$\begin{aligned} \mu^2(T) &= \frac{\eta m \Omega}{2\hbar} \coth \left(\frac{\hbar \Omega}{4kT} \right), \\ \nu^2(T) &= \frac{\eta}{2\hbar m \Omega} \tanh \left(\frac{\hbar \Omega}{4kT} \right) \end{aligned} \quad (14)$$

with the accompanying relation $2\mu\nu\hbar = \eta$, and k is the Boltzmann constant, T is the temperature, $\eta > 0$ is the characteristic damping rate.

This Lindblad equation can be written out explicitly according to Eq. (12) and Eq. (13),

$$\frac{d\rho}{dt} + \frac{i}{\hbar} [H', \rho] = -\mu^2 [x, [x, \rho]] - 2i\mu\nu [x, [p, \rho]]_+$$

$$-\nu^2 [p, [p, \rho]], \quad (15)$$

where $H' = H - 2\mu\nu\hbar xp$. We also call this equation the Lindblad equation of **Quantum Langevin Dynamics**, abbreviated as **QLD**, which is also the name of our algorithm. The coordinate space representation of Eq. (15) [41] is also used in the numerical experiments of QLD, stated here for completeness:

$$\begin{aligned} \frac{\partial \rho(x, y, t)}{\partial t} + \frac{i}{\hbar} [\tilde{H}(x) - \tilde{H}^*(y)] \rho(x, y, t) = & - \left(\mu^2(T) (x - y)^2 + \eta (x - y) \left(\frac{\partial}{\partial x} - \frac{\partial}{\partial y} \right) \right. \\ & \left. - \nu^2(T) \hbar^2 \left(\frac{\partial}{\partial x} + \frac{\partial}{\partial y} \right)^2 \right) \rho(x, y, t), \end{aligned} \quad (16)$$

where $\tilde{H}(x) = H(x) + i\hbar\eta x \frac{\partial}{\partial x} + i\frac{\hbar\eta}{2}$.

III. CONVERGENCE OF QLD

In this section, our primary focus is the time-independent scenario of QLD, implying that all parameters $\eta, \hbar, T, m, \Omega, k$ remain constant throughout evolution. In the convex case, the convergence rate of QLD is $O(e^{-\eta t})$ as demonstrated in Theorem 1. Subsequently, we compute the analytical solution of the quadratic potential, the simplest convex function, in Section III B. The most remarkable discovery related to the quadratic potential is that the system will reach the ground state of the quadratic potential when the evolution time $t \rightarrow +\infty$ and the temperature $T \rightarrow 0$. Lastly, we prove that QLD continues to converge to the global minimum even in a specific nonconvex scenario, where the objective function satisfies $x \cdot \nabla V(x) \geq rV(x) \geq 0$ for $r \in (0, 1)$, at a rate of $O(e^{-\eta t})$. More details can be referred to Theorem 2 of Section III C.

A. Convergence of QLD in the convex case

Our goal is to demonstrate that the expectation value of the objective function $V(x)$ converges to the global minimum $V(x^*)$ at a defined rate under the evolution of QLD. This necessitates the consideration of the expectation value of the Hamiltonian H , as if we can establish that the expectation value of H diminishes, it follows that the expectation value of V will also decrease. With this understanding, we initially present Lemma 1, which enables us to calculate the time evolution of the expectation value of any observable evolving by standard Lindblad equation. After that, we show some commutation relations used in the calculation referring to Lemma 2. Subsequently, we verify the convergence of the expectation value of H in Proposition 2, and with the assistance

of this proposition, we validate the convergence of the expectation value of V in Theorem 1.

Theorem 1 (Convergence of QLD). *Assume that V is a continuously differentiable convex function and $\nabla^2 V(x) < +\infty$ for any x in the domain. Let x^* be the unique global minimum of $V(x)$. Then the solution $\rho(t)$ to Eq. (15), with approximation $\hbar\Omega \ll kT$, satisfies that*

$$\langle V \rangle_t - V(x^*) \leq 2kT + O(e^{-\eta t}), \quad (17)$$

if the initial density matrix $\rho(0)$ satisfies $\langle H \rangle_0 - 2kT \geq 0$, where $\langle \cdot \rangle_t$ denotes the expectation value with respect to the density matrix $\rho(t)$, i.e., $\langle \cdot \rangle_t = \text{Tr}(\cdot \rho(t))$.

Proof. Without loss of generality, we can position the global minimum of V at the origin by shifting the function vertically and horizontally, which derives $x^* = 0$ and $V(x^*) = 0$. Then we only need to prove

$$\langle V \rangle_t \leq 2kT + O(e^{-\eta t}). \quad (18)$$

Because $\langle \frac{p^2}{2m} \rangle_t + \langle V \rangle_t = \langle H \rangle_t$ and all these three terms are greater than or equal to zero, we have

$$\langle V \rangle_t \leq \langle H \rangle_t. \quad (19)$$

By Proposition 2, we get $\langle V \rangle_t \leq \langle H \rangle_t \leq 2kT + O(e^{-\eta t})$. \square

Remark 1. *If the desired accuracy is ε , which means we want $\langle V \rangle_t - V(x^*) \leq \varepsilon$ when $t \rightarrow +\infty$. To achieve this, we only need to set $kT = \varepsilon/2$ and ensure the approximation $\hbar\Omega \ll kT$ still holds.*

Lemma 1 (Generalized Ehrenfest theorem). *Given a time-dependent quantum observable $O(t)$ and let $\rho(t)$ be the solution of the standard Lindblad equation Eq. (12). Then the time derivative of the expectation value of $O(t)$ is given by*

$$\frac{d}{dt} \langle O(t) \rangle_t = \left\langle \frac{d}{dt} O(t) \right\rangle_t + \frac{i}{\hbar} \langle [H, O(t)] \rangle_t$$

$$+ \sum_{j=1}^m \left\langle \left(-L_j^\dagger [L_j, O(t)] + [L_j^\dagger, O(t)] L_j \right) \right\rangle_t. \quad (20)$$

Proof.

$$\begin{aligned} \frac{d}{dt} \langle O(t) \rangle_t &= \frac{d}{dt} \text{Tr}(O(t)\rho(t)) \\ &= \text{Tr} \left(\frac{dO(t)}{dt} \rho(t) \right) + \text{Tr} \left(O(t) \frac{d\rho(t)}{dt} \right) \\ &= \left\langle \frac{d}{dt} O(t) \right\rangle_t + \text{Tr} \left(O(t) \frac{d\rho(t)}{dt} \right). \end{aligned} \quad (21)$$

Let's focus on the second term $\text{Tr} \left(O(t) \frac{d\rho(t)}{dt} \right)$. Inserting Eq. (12) into the second term, we get

$$\begin{aligned} &\text{Tr} \left(O(t) \frac{d\rho(t)}{dt} \right) \\ &= \text{Tr} \left(-\frac{i}{\hbar} O(t) [H, \rho(t)] \right. \\ &\quad \left. + \sum_{j=1}^m O(t) \left(2L_j \rho(t) L_j^\dagger - L_j^\dagger L_j \rho(t) - \rho(t) L_j^\dagger L_j \right) \right) \\ &= -\frac{i}{\hbar} \text{Tr} (O(t) [H, \rho(t)]) \\ &\quad + \text{Tr} \left(\sum_{j=1}^m O(t) \left(2L_j \rho(t) L_j^\dagger - L_j^\dagger L_j \rho(t) - \rho(t) L_j^\dagger L_j \right) \right), \end{aligned} \quad (22)$$

where the first term $\text{Tr} (O(t) [H, \rho(t)])$ could be simplified as follows:

$$\begin{aligned} \text{Tr} (O(t) [H, \rho(t)]) &= \text{Tr} (OH\rho) - \text{Tr} (O\rho H) \\ &= \text{Tr} (OH\rho) - \text{Tr} (HO\rho) \\ &= \text{Tr} ([O, H]\rho) \\ &= -\langle [H, O] \rangle_t. \end{aligned} \quad (23)$$

The second term of Eq. (22) becomes

$$\begin{aligned} &\sum_{j=1}^m \text{Tr} \left(O(t) \left(2L_j \rho(t) L_j^\dagger - L_j^\dagger L_j \rho(t) - \rho(t) L_j^\dagger L_j \right) \right) \\ &= \sum_{j=1}^m \text{Tr} \left(O(t) 2L_j \rho(t) L_j^\dagger \right) - \sum_{j=1}^m \text{Tr} \left(O(t) L_j^\dagger L_j \rho(t) \right) \\ &\quad - \sum_{j=1}^m \text{Tr} \left(O(t) \rho(t) L_j^\dagger L_j \right) \\ &= \sum_{j=1}^m \text{Tr} \left(2L_j^\dagger O(t) L_j \rho(t) \right) - \sum_{j=1}^m \text{Tr} \left(O(t) L_j^\dagger L_j \rho(t) \right) \\ &\quad - \sum_{j=1}^m \text{Tr} \left(L_j^\dagger L_j O(t) \rho(t) \right) \\ &= \sum_{j=1}^m \text{Tr} \left(\left(2L_j^\dagger O(t) L_j - O(t) L_j^\dagger L_j - L_j^\dagger L_j O(t) \right) \rho(t) \right) \end{aligned}$$

$$\begin{aligned} &= \sum_{j=1}^m \text{Tr} \left(\left(-L_j^\dagger [L_j, O(t)] + [L_j^\dagger, O(t)] L_j \right) \rho(t) \right) \\ &= \sum_{j=1}^m \left\langle \left(-L_j^\dagger [L_j, O(t)] + [L_j^\dagger, O(t)] L_j \right) \right\rangle_t. \end{aligned} \quad (24)$$

Inserting Eq. (22), Eq. (23) and Eq. (24) into Eq. (21), we complete the proof. \square

Lemma 2 (Commutation relations). *Let x and p be the position operator and momentum operator, respectively. f is any continuously differentiable function. Then*

$$[x, p^2] = 2i\hbar p, \quad (25a)$$

$$[f(x), p] = i\hbar \nabla f, \quad (25b)$$

$$[\nabla f(x), p] = i\hbar \nabla^2 f, \quad (25c)$$

$$[f(x), p^2] = i\hbar [\nabla f, p]_+, \quad (25d)$$

$$[p, xp] = [p, px] = -i\hbar p, \quad (25e)$$

$$[x, px] = [x, xp] = i\hbar x, \quad (25f)$$

$$[p^2, xp] = [p^2, px] = -2i\hbar p^2, \quad (25g)$$

$$[x^2, xp] = [x^2, px] = 2i\hbar x^2. \quad (25h)$$

Proof. It is well-known that $[x, p] = i\hbar$ [47].

$$[x, p^2] = xp^2 - p^2x = p[x, p] + [x, p]p = 2i\hbar p$$

In order to prove Eq. (25b), we introduce a continuously differentiable test function $g(x)$, then

$$\begin{aligned} [f, p]g &= \left(f \frac{\hbar}{i} \nabla - \frac{\hbar}{i} \nabla f \right) g \\ &= \frac{\hbar}{i} (f \nabla g - \nabla f g) \\ &= \frac{\hbar}{i} (f \nabla g - f \nabla g - g \nabla f) \\ &= i\hbar g \nabla f, \end{aligned}$$

so we get $[f(x), p] = i\hbar \nabla f$.

Similarly, we have $[\nabla f(x), p] = i\hbar \nabla^2 f$.

$$\begin{aligned} [f(x), p^2] &= f(x)p^2 - p^2f(x) \\ &= p[f, p] + [f, p]p \\ &= p \cdot i\hbar \nabla f + i\hbar \nabla f \cdot p \\ &= i\hbar [\nabla f, p]_+. \end{aligned}$$

$$[p, xp] = -[xp, p] = -x[p, p] - [x, p]p = -i\hbar p.$$

Similarly, we can prove $[p, px] = -i\hbar p$ and $[x, px] = [x, xp] = i\hbar x$.

$$\begin{aligned} [p^2, xp] &= p[p, xp] + [p, xp]p \\ &= -p \cdot i\hbar p - i\hbar p \cdot p \\ &= -2i\hbar p^2. \end{aligned}$$

Similarly, we can show that $[p^2, px] = -2i\hbar p^2$ and $[x^2, xp] = [x^2, px] = 2i\hbar x^2$. \square

Proposition 1. *If $\lim_{x \rightarrow \infty} V(x) = +\infty$, there always exists an initial density matrix $\rho(0)$ that satisfies $\langle H \rangle_0 > R$, for any $R \in \mathbb{R}, R > 0$.*

Proof. This proof is quite straightforward. We only need to ensure the initial density matrix $\rho(0)$ is heavily weighted in the region where V is large to realize $\langle V \rangle_0 > R$. Because $\langle V \rangle_0 \leq \langle H \rangle_0$, we have $\langle H \rangle_0 > R$. \square

Proposition 2. *Assume that V is a continuously differentiable convex function and $\nabla^2 V(x) < +\infty$ for any x in the domain. If $\hbar\Omega \ll kT$ and the initial condition satisfies $\langle H \rangle_0 - 2kT > 0$, the inequality $\langle H \rangle_t - 2kT \leq (\langle H \rangle_0 - 2kT)e^{-\eta t} = O(e^{-\eta t})$ holds under the evolution of Eq. (15).*

Proof. Without loss of generality, we still set $x^* = 0$ and $V(x^*) = 0$. By Lemma 1, we have

$$\begin{aligned} \frac{d}{dt} \langle H \rangle_t &= \left\langle \frac{d}{dt} H \right\rangle_t + \frac{i}{\hbar} \langle [H, H] \rangle_t \\ &\quad + \langle -L^\dagger [L, H] + [L^\dagger, H] L \rangle_t. \end{aligned} \quad (26)$$

The first and second terms are zero, so we only need to calculate the third term. Inserting Eq. (13) into the third term, we get

$$\begin{aligned} &\langle -L^\dagger [L, H] + [L^\dagger, H] L \rangle_t \\ &= \langle -L^\dagger [\mu x + i\nu p, p^2/(2m) + V] \\ &\quad + [\mu x - i\nu p, p^2/(2m) + V] L \rangle_t \\ &= \left\langle -L^\dagger \left(\frac{\mu}{2m} [x, p^2] + \mu [x, V] + i \frac{\nu}{2m} [p, p^2] + i\nu [p, V] \right) \right. \\ &\quad \left. + \left(\frac{\mu}{2m} [x, p^2] + \mu [x, V] - i \frac{\nu}{2m} [p, p^2] - i\nu [p, V] \right) L \right\rangle_t \\ &= \left\langle (-\mu x + i\nu p) \left(i \frac{\mu}{m} \hbar p + \nu \hbar \nabla V \right) \right. \\ &\quad \left. + \left(i \frac{\mu}{m} \hbar p - \nu \hbar \nabla V \right) (\mu x + i\nu p) \right\rangle_t \\ &= \left\langle -i \frac{\mu^2}{m} \hbar (xp - px) - 2\mu\nu \hbar (x \cdot \nabla V + p^2/m) \right\rangle_t \\ &\quad + \langle i\nu^2 \hbar (p \cdot \nabla V - \nabla V \cdot p) \rangle_t \\ &= \left\langle -i \frac{\mu^2}{m} \hbar [x, p] - 2\mu\nu \hbar (x \cdot \nabla V + p^2/m) + i\nu^2 \hbar [p, \nabla V] \right\rangle_t \\ &= \left\langle \frac{\mu^2}{m} \hbar^2 - 2\mu\nu \hbar (x \cdot \nabla V + p^2/m) + \nu^2 \hbar^2 \nabla^2 V \right\rangle_t \\ &= \hbar^2 \left(\frac{\mu^2}{m} + \nu^2 \langle \nabla^2 V \rangle_t \right) - 2\mu\nu \hbar \langle x \cdot \nabla V + p^2/m \rangle_t. \end{aligned} \quad (27)$$

In the above derivations, Lemma 2 is also used to simplify.

Known that $2\hbar\mu\nu = \eta$, put this into the above equation, then we get

$$\frac{d}{dt} \langle H \rangle_t = \hbar^2 \left(\frac{\mu^2}{m} + \nu^2 \langle \nabla^2 V \rangle_t \right) - 2\mu\nu \hbar \langle x \cdot \nabla V + p^2/m \rangle_t \quad (28a)$$

$$= \left(\frac{\hbar^2 \mu^2}{m} + \frac{\eta^2}{4\mu^2} \langle \nabla^2 V \rangle_t \right) - \eta \langle x \cdot \nabla V + p^2/m \rangle_t. \quad (28b)$$

According to the approximation $\hbar\Omega \ll kT$, Eq. (14) becomes

$$\mu^2 = \frac{\eta m \Omega}{2\hbar} \left(\frac{4kT}{\hbar\Omega} + \frac{\hbar\Omega}{12kT} + O\left(\left(\frac{\hbar\Omega}{kT}\right)^3\right) \right), \quad (29)$$

$$\frac{1}{\mu^2} = \frac{2\hbar}{\eta m \Omega} \left(\frac{\hbar\Omega}{4kT} + O\left(\left(\frac{\hbar\Omega}{kT}\right)^3\right) \right). \quad (30)$$

Inserting the above equations into Eq. (28b), Eq. (28b) becomes

$$\begin{aligned} \frac{d}{dt} \langle H \rangle_t &= \eta \cdot 2kT + \eta \cdot \frac{\hbar\Omega}{kT} \left(\frac{\hbar\Omega}{24} + \frac{\hbar}{8m\Omega} \langle \nabla^2 V \rangle_t \right) \\ &\quad + O\left(\left(\frac{\hbar\Omega}{kT}\right)^3\right) - \eta \langle x \cdot \nabla V + p^2/m \rangle_t. \end{aligned} \quad (31)$$

The assumption $\nabla^2 V(x) < +\infty$ and approximation $\frac{\hbar\Omega}{kT} \ll 1$ guarantee that $\eta \cdot \frac{\hbar\Omega}{kT} \cdot \frac{\hbar}{8m\Omega} \langle \nabla^2 V \rangle_t$ is negligible compared to $\eta \cdot 2kT$, which also tells us how small $\frac{\hbar\Omega}{kT}$ must be at least to ensure the approximation work. Neglecting all higher order terms, we get

$$\frac{d}{dt} \langle H \rangle_t = \eta \cdot (2kT - \langle x \cdot \nabla V + p^2/m \rangle_t) \quad (32)$$

$$\begin{aligned} &\leq \eta \cdot (2kT - \langle x \cdot \nabla V + p^2/(2m) \rangle_t) \\ &\leq \eta \cdot (2kT - \langle V + p^2/(2m) \rangle_t), \end{aligned} \quad (33)$$

where the last inequality comes from the property of convex functions $x \cdot \nabla V(x) \geq V(x) \geq 0$. Finally, we have

$$\frac{d}{dt} \langle H \rangle_t \leq \eta \cdot (2kT - \langle H \rangle_t). \quad (34)$$

Construct a function $h(t) = (\langle H \rangle_t - 2kT)e^{\eta t}$, and it is direct to verify that $\frac{dh(t)}{dt} \leq 0$ for $\forall t > 0$ by Eq. (34). Consequently, we get $h(t) \leq h(0)$,

$$\langle H \rangle_t - 2kT \leq (\langle H \rangle_0 - 2kT)e^{-\eta t} = O(e^{-\eta t}). \quad (35)$$

\square

B. Analytical solution with quadratic potentials

It is intractable to solve the Lindblad equation of QLD Eq. (15) analytically in most cases. However, we can solve it analytically for quadratic potentials. Here, we consider the simplest one-dimensional case with quadratic potential $V(x) = \frac{1}{2}m\Omega^2 x^2$, which also implies that the system is a harmonic oscillator with energy level $\mathcal{H}_k = (\frac{1}{2} + k)\hbar\Omega$ ($k = 0, 1, \dots$). For the multidimensional scenario where $V(\mathbf{x}) = \frac{1}{2}x^T \mathbf{A}x$ with a positive semidefinite matrix \mathbf{A} , it can be solved by the normal mode

analysis method (regularization) [48]. In the following part, we mainly calculate the time evolutions of expectation value of kinetic energy $\langle \frac{p^2}{2m} \rangle_t$ and potential energy $\langle V \rangle_t$. An interesting thing we find is that the system always reaches the ground state of harmonic oscillator with ground state energy $\mathcal{H}_0 = \frac{1}{2}\hbar\Omega$ if $T \rightarrow 0$ when $t \rightarrow +\infty$, no matter what initial density matrix $\rho(0)$ we set.

At first, we need to calculate $\frac{d}{dt}\langle V \rangle_t$ similar to the previous calculation of $\frac{d}{dt}\langle H \rangle_t$ in Proposition 2. By Lemma 1 and Lemma 2, we have

$$\begin{aligned}
& \frac{d}{dt}\langle V \rangle_t \\
&= \left\langle \frac{d}{dt} V \right\rangle_t + \frac{i}{\hbar} \langle [H, V] \rangle_t + \langle -L^\dagger [L, V] + [L^\dagger, V] L \rangle_t \\
&= \frac{i}{\hbar} \langle [p^2/(2m) + V, V] \rangle_t \\
&\quad + \langle -L^\dagger [\mu x + i\nu p, V] + [\mu x - i\nu p, V] L \rangle_t \\
&= \frac{i}{\hbar} \langle [p^2/(2m), V] + [V, V] \rangle_t + \langle -L^\dagger (\mu [x, V] + i\nu [p, V]) \\
&\quad + (\mu [x, V] - i\nu [p, V]) L \rangle_t \\
&= \frac{i}{2m\hbar} \langle [p^2, V] \rangle_t + \langle -L^\dagger i\nu [p, V] - i\nu [p, V] L \rangle_t \\
&= \frac{i}{2m\hbar} \langle -i\hbar [\nabla V, p]_+ \rangle_t \\
&\quad + \langle (-\mu x + i\nu p)\nu\hbar\nabla V - \nu\hbar\nabla V(\mu x + i\nu p) \rangle_t \\
&= \frac{1}{2m} \langle [\nabla V, p]_+ \rangle_t - 2\mu\nu\hbar \langle x \cdot \nabla V \rangle_t + \hbar^2\nu^2 \langle \nabla^2 V \rangle_t. \quad (36)
\end{aligned}$$

Then, inserting $V(x) = \frac{1}{2}m\Omega^2 x^2$ into above equation and implementing Lemma 2 again, we get

$$\begin{aligned}
\frac{d}{dt}\langle x^2 \rangle_t &= \frac{1}{m} \langle [x, p]_+ \rangle_t - 4\mu\nu\hbar \langle x^2 \rangle_t + 2\hbar^2\nu^2 \\
&= \frac{1}{m} \langle [x, p]_+ \rangle_t - 2\eta \langle x^2 \rangle_t + 2\hbar^2\nu^2. \quad (37)
\end{aligned}$$

From Eq. (28b), we have

$$\begin{aligned}
& \frac{d}{dt} \left\langle \frac{p^2}{2m} + \frac{1}{2}m\Omega^2 x^2 \right\rangle_t \\
&= \hbar^2 \left(\frac{\mu^2}{m} + \nu^2 m\Omega^2 \right) - \eta \langle m\Omega^2 x^2 + p^2/m \rangle_t. \quad (38)
\end{aligned}$$

Eq. (38) minus Eq. (37):

$$\frac{d}{dt}\langle p^2 \rangle_t = -m\Omega^2 \langle [x, p]_+ \rangle_t - 2\eta \langle p^2 \rangle_t + 2\hbar^2\mu^2. \quad (39)$$

Observing that the time differential equations of $\langle x^2 \rangle_t$ and $\langle p^2 \rangle_t$ have been collected in Eq. (37) and Eq. (39), if we want to formulate a complete set of differential equations, time differential equation of $\langle [x, p]_+ \rangle_t$ must be obtained. By Lemma 1 and Lemma 2, we can calculate

$$\frac{d}{dt} \langle [x, p]_+ \rangle_t = \left\langle \frac{d}{dt} [x, p]_+ \right\rangle_t + \frac{i}{\hbar} \langle [H, [x, p]_+] \rangle_t$$

$$+ \langle -L^\dagger [L, [x, p]_+] + [L^\dagger, [x, p]_+] L \rangle_t, \quad (40)$$

where

$$\begin{aligned}
& \langle [H, [x, p]_+] \rangle_t \\
&= \left\langle \left[\frac{p^2}{2m} + \frac{1}{2}m\Omega^2 x^2, [x, p]_+ \right] \right\rangle_t \\
&= \frac{1}{2m} \langle [p^2, [x, p]_+] \rangle_t + \frac{1}{2}m\Omega^2 \langle [x^2, [x, p]_+] \rangle_t \\
&= \frac{1}{2m} \langle -4i\hbar p^2 \rangle_t + \frac{1}{2}m\Omega^2 \langle 4i\hbar x^2 \rangle_t \\
&= \frac{-2i\hbar}{m} \langle p^2 \rangle_t + 2i\hbar m\Omega^2 \langle x^2 \rangle_t \quad (41)
\end{aligned}$$

and

$$\begin{aligned}
& \langle -L^\dagger [L, [x, p]_+] + [L^\dagger, [x, p]_+] L \rangle_t \\
&= \langle -L^\dagger [\mu x + i\nu p, [x, p]_+] + [\mu x - i\nu p, [x, p]_+] L \rangle_t \\
&= \langle -L^\dagger (\mu [x, [x, p]_+] + i\nu [p, [x, p]_+]) \rangle_t \\
&\quad + \langle (\mu [x, [x, p]_+] - i\nu [p, [x, p]_+]) L \rangle_t \\
&= \langle -L^\dagger (2i\mu\hbar x + 2\nu\hbar p) \rangle_t + \langle (2i\mu\hbar x - 2\nu\hbar p) L \rangle_t \\
&= \langle -(\mu x - i\nu p) (2i\mu\hbar x + 2\nu\hbar p) \rangle_t \\
&\quad + \langle (2i\mu\hbar x - 2\nu\hbar p) (\mu x + i\nu p) \rangle_t \\
&= -4\hbar\mu\nu \langle [x, p]_+ \rangle_t \\
&= -2\eta \langle [x, p]_+ \rangle_t. \quad (42)
\end{aligned}$$

Inserting Eq. (41) and Eq. (42) into Eq. (40):

$$\frac{d}{dt} \langle [x, p]_+ \rangle_t = \frac{2}{m} \langle p^2 \rangle_t - 2m\Omega^2 \langle x^2 \rangle_t - 2\eta \langle [x, p]_+ \rangle_t. \quad (43)$$

For convenience, we restate all three equations together here

$$\frac{d}{dt} \langle x^2 \rangle_t = \frac{1}{m} \langle [x, p]_+ \rangle_t - 2\eta \langle x^2 \rangle_t + 2\hbar^2\nu^2, \quad (44a)$$

$$\frac{d}{dt} \langle [x, p]_+ \rangle_t = \frac{2}{m} \langle p^2 \rangle_t - 2m\Omega^2 \langle x^2 \rangle_t - 2\eta \langle [x, p]_+ \rangle_t, \quad (44b)$$

$$\frac{d}{dt} \langle p^2 \rangle_t = -m\Omega^2 \langle [x, p]_+ \rangle_t - 2\eta \langle p^2 \rangle_t + 2\hbar^2\mu^2, \quad (44c)$$

which form a complete group of differential equations. Eq. (44a) gives

$$\frac{1}{m} \langle [x, p]_+ \rangle_t = \frac{d}{dt} \langle x^2 \rangle_t + 2\eta \langle x^2 \rangle_t - 2\hbar^2\nu^2. \quad (45)$$

Inserting it into Eq. (44b), then $\langle p^2 \rangle_t$ can be presented as a function of $\langle x^2 \rangle_t$ and its time derivatives

$$\begin{aligned}
\langle p^2 \rangle_t &= \frac{m^2}{2} \frac{d^2}{dt^2} \langle x^2 \rangle_t + 2m^2\eta \frac{d}{dt} \langle x^2 \rangle_t \\
&\quad + m^2 (2\eta^2 + \Omega^2) \langle x^2 \rangle_t - 2\hbar^2\nu^2 m^2. \quad (46)
\end{aligned}$$

Finally, we insert Eq. (45) and the time derivative of Eq. (46) into Eq. (44c), which gives

$$\frac{d^3 \langle x^2 \rangle_t}{dt^3} + 6\eta \frac{d^2 \langle x^2 \rangle_t}{dt^2} + (4\Omega^2 + 12\eta^2) \frac{d \langle x^2 \rangle_t}{dt}$$

$$+8\eta(\Omega^2 + \eta^2)\langle x^2 \rangle_t - D = 0, \quad (47)$$

where D is a constant

$$D = \frac{4}{m^2}\mu^2\hbar^2 + 4(\Omega^2 + 2\eta^2)\nu^2\hbar^2. \quad (48)$$

The analytical solution of Eq. (47) is

$$\begin{aligned} \langle x^2 \rangle_t &= e^{-2\eta t} (A + B e^{2i\Omega t} + C e^{-2i\Omega t}) + \frac{D}{8\eta(\Omega^2 + \eta^2)} \\ &= e^{-2\eta t} (A + \tilde{B} \cos(2\Omega t) + \tilde{C} \sin(2\Omega t)) \\ &\quad + \frac{D}{8\eta(\Omega^2 + \eta^2)}, \end{aligned} \quad (49)$$

where A, B, C are three constants determined by the initial condition of the system and $A, \tilde{B}, \tilde{C} \in \mathbb{R}$. This also means that the convergence rate of $\langle V(x) \rangle_t = \frac{1}{2}m\Omega^2 \langle x^2 \rangle_t$ is $O(e^{-2\eta t})$.

Calculating the time derivatives of Eq. (49), we have

$$\begin{aligned} \frac{d}{dt} \langle x^2 \rangle_t &= e^{-2\eta t} (-2\eta A + 2 \cos(2\Omega t)(-\eta \tilde{B} + \Omega \tilde{C}) \\ &\quad + 2 \sin(2\Omega t)(-\Omega \tilde{B} - \eta \tilde{C})), \end{aligned} \quad (50)$$

and

$$\begin{aligned} \frac{d^2}{dt^2} \langle x^2 \rangle_t &= e^{-2\eta t} (4\eta^2 A + 4 \cos(2\Omega t)(\eta^2 \tilde{B} - \Omega^2 \tilde{B} - 2\eta \Omega \tilde{C}) \\ &\quad + 4 \sin(2\Omega t)(\eta^2 \tilde{C} - \Omega^2 \tilde{C} + 2\eta \Omega \tilde{B})). \end{aligned} \quad (51)$$

Inserting the above two equations into Eq. (46), we get

$$\begin{aligned} \left\langle \frac{p^2}{m^2} \right\rangle_t &= e^{-2\eta t} (A\Omega^2 - \Omega^2 \tilde{B} \cos(2\Omega t) - \Omega^2 \tilde{C} \sin(2\Omega t)) \\ &\quad + \frac{(2\eta^2 + \Omega^2)D}{8\eta(\Omega^2 + \eta^2)} - 2\hbar^2\nu^2\eta. \end{aligned} \quad (52)$$

When $t \rightarrow +\infty$, the convergence value of average potential is

$$\langle V \rangle_f = \frac{1}{2}m\Omega^2 \langle x^2 \rangle_{t \rightarrow +\infty} \rightarrow \frac{1}{2}m\Omega^2 \frac{D}{8\eta(\Omega^2 + \eta^2)}. \quad (53)$$

When $T \rightarrow 0$ and $t \rightarrow +\infty$, $\langle V \rangle_f = \langle \frac{1}{2}m\Omega^2 x^2 \rangle_t \rightarrow \frac{1}{4}\hbar\Omega$.

When $t \rightarrow +\infty$, the convergence value of average kinetic energy is

$$\langle E_k \rangle_f = \left\langle \frac{p^2}{2m} \right\rangle_{t \rightarrow +\infty} \rightarrow \frac{m(2\eta^2 + \Omega^2)D}{16\eta(\Omega^2 + \eta^2)} - m\hbar^2\nu^2\eta. \quad (54)$$

When $T \rightarrow 0$ and $t \rightarrow +\infty$, $\langle E_k \rangle_f = \left\langle \frac{p^2}{2m} \right\rangle_{t \rightarrow +\infty} \rightarrow \frac{1}{4}\hbar\Omega$. The above evidences suggest the system reaches the ground state of energy level $\mathcal{H}_0 = \frac{1}{2}\hbar\Omega$.

We can also view this fact from another point of view. Inserting Eq. (14) into Eq. (38), the time derivative of $\langle H \rangle_t$ is

$$\begin{aligned} \frac{d\langle H \rangle_t}{dt} &= -\eta \left\langle m\Omega^2 x^2 + \frac{p^2}{m} \right\rangle_t + \frac{1}{2}\eta\Omega\hbar \coth\left(\frac{\hbar\Omega}{4kT}\right) \\ &\quad + \frac{1}{2}\eta\Omega\hbar \tanh\left(\frac{\hbar\Omega}{4kT}\right) \\ &= -2\eta \langle H \rangle_t + \eta\hbar\Omega \coth\left(\frac{\hbar\Omega}{2kT}\right). \end{aligned} \quad (55)$$

Trying to present the energy level of the system by a time-dependent energy level number n_t ($n_t \in \mathbb{R}$), we have $\langle H \rangle_t = (n_t + 1/2)\hbar\Omega$. The evolution of n_t indicates the energy level transition of the system. Then Eq. (55) becomes

$$\frac{d\langle H \rangle_t}{dt} = \left(-2n_t - 1 + \coth\left(\frac{\hbar\Omega}{2kT}\right) \right) \eta\hbar\Omega. \quad (56)$$

When $n_t > \frac{1}{2}(\coth(\frac{\hbar\Omega}{2kT}) - 1)$, $\frac{d\langle H \rangle_t}{dt} < 0$ makes n_t keep decreasing until $n_t \rightarrow \frac{1}{2}(\coth(\frac{\hbar\Omega}{2kT}) - 1)$. Unless the temperature is extremely small ($T \rightarrow 0 \Rightarrow \coth(\frac{\hbar\Omega}{2kT}) \rightarrow 1^+$), the system cannot reach the ground state.

C. Convergence of QLD in the nonconvex case

For general nonconvex potential, we cannot prove the convergence of QLD. However, when facing some special nonconvex ones, QLD can still converge to the global minimum within desired precision. Consider a special example of a one-dimensional nonconvex potential:

$$V(x) = \begin{cases} 2m\Omega^2\delta^{3/2}\sqrt{|x|} - \frac{3}{2}m\Omega^2\delta^2, & |x| \in (\delta, +\infty) \\ \frac{1}{2}m\Omega^2x^2, & x \in [-\delta, \delta] \end{cases}$$

where $\delta > 0$ is constant. This potential is a nonconvex function, which is also continuously differentiable. We find QLD can still converge to the global minimum within desired precision in this case. Noticing this function satisfies $x \cdot \nabla V \geq 0.5V(x) \geq 0$, we can generalize it to get a more general nonconvex potential which satisfies $x \cdot \nabla V \geq rV(x) \geq 0$ for a constant $r \in (0, 1)$. Here, we still assume this kind of potential is continuously differentiable with unique global minimum $x^* = 0$ and $V(x^*) = 0$. We call this case slightly nonconvex case.

In this case, we establish the following convergence rate of QLD by applying similar proof techniques to Theorem 1.

Theorem 2 (Convergence of QLD in slight-nonconvexity case). *Assume that V is a continuously differentiable function, which satisfies $\nabla^2 V(x) < +\infty$ and $x \cdot \nabla V(x) \geq rV(x) \geq 0$, where $r \in (0, 1)$ is a constant. Let x^* be the unique global minimum of $V(x)$. Then the solution $\rho(t)$ to Eq. (15), with approximation $\hbar\Omega \ll kT$, satisfies that*

$$\langle V(x) \rangle_t - V(x^*) \leq \frac{2}{r}kT + O(e^{-\eta rt}), \quad (57)$$

if the initial density matrix $\rho(0)$ satisfies $\langle H \rangle_0 - \frac{2}{r}kT \geq 0$.

Proof. Without loss of generality, we assume $x^* = 0$ and $V(x^*) = 0$. Then we only need to prove

$$\langle V(x) \rangle_t \leq \frac{2}{r}kT + O(e^{-\eta rt}). \quad (58)$$

In this case, Eq. (32) still holds with approximation $\hbar\Omega \ll kT$ and assumption $\nabla^2 V(x) < +\infty$. With the constraint $x \cdot \nabla V(x) \geq rV(x) \geq 0$, Eq. (32) becomes

$$\begin{aligned} \frac{d}{dt} \langle H \rangle_t &= \eta \cdot (2kT - \langle x \cdot \nabla V + p^2/m \rangle_t) \\ &\leq \eta \cdot (2kT - \langle rV + p^2/m \rangle_t) \\ &= \eta \cdot \left(2kT - \left\langle r(V(x) + \frac{p^2}{2m}) + (1 - \frac{r}{2}) \frac{p^2}{m} \right\rangle_t \right) \\ &\leq -\eta r \langle H(x) \rangle_t + 2\eta kT. \end{aligned} \quad (59)$$

Let $h(t) = (\langle H \rangle_t - \frac{2}{r}kT)e^{\eta rt}$, then verify that $\frac{dh(t)}{dt} \leq 0$ for $\forall t > 0$ by Eq. (59). Consequently, we get $h(t) \leq h(0)$,

$$\langle H(x) \rangle_t - \frac{2}{r}kT \leq \left(\langle H \rangle_0 - \frac{2}{r}kT \right) e^{-\eta rt} = O(e^{-\eta rt}). \quad (60)$$

Hence we have

$$\langle V(x) \rangle_t \leq \langle H \rangle_t \leq \frac{2}{r}kT + O(e^{-\eta rt}). \quad (61)$$

□

Remark 2. To achieve a desired accuracy ε , i.e., $\langle V \rangle_t - V(x^*) \leq \varepsilon$ when $t \rightarrow +\infty$, we only need to set $kT = r\varepsilon/2$ and ensure that the approximation $\hbar\Omega \ll kT$ still holds.

IV. NUMERICAL RESULTS OF TIME-INDEPENDENT QLD

In this section, we conduct numerical experiments for time-independent QLD, i.e., all parameters remain constant throughout the evolution. In Section IV A, we initially delve into the origin of dissipation, grounding our understanding in the intuitive concept of spontaneous emission. Section IV A also demonstrates that spontaneous emission can endow the system with the ability to transit to the ground state and achieve stability as the size of the heat bath increases. Section IV B primarily discusses the numerical methods employed to solving QLD. These technical details are essential for maintaining numerical stability during numerical computation. We then employ numerical experiments to validate the theoretical results concerning the quadratic potential from Section III B, as detailed in Section IV C. In the experiments of the quadratic potential, we found that the numerical results are in alignment with the theoretical predictions. This consistency validates the precision of

our numerical experiments. Subsequently, roles of each parameter in QLD are individually discussed in Section IV D. We discover that the parameter η influences the speed of convergence in QLD, while the magnitudes of \hbar and T impact the system's ability to escape from local minima. Finally, Section IV E presents a comparison of the performance between the time-independent QLD and its classical counterpart, the Fokker-Planck-Smoluchowski equation. This comparison demonstrates the consistency of the classical and quantum thermal effects.

All results and plots are obtained by simulations on classical computers (Intel® Core™ i9-13900KS Processor with 128GB memory) via MATLAB 2023a, also including numerical experiments in Section V.

A. Verification of the intuition: spontaneous emission

QLD describes the dynamics when the number of oscillators in heat bath is infinite. The essential cause of energy dissipation in QLD can trace back to spontaneous emission in quantum mechanics [49]. Intuitively, we have an assumption: the system has the ability to escape from local minimum as long as the number of oscillators in heat bath is finite.

We utilize a specific numerical case to support our assumption. We choose a new landscape, an asymmetric quadratic potential

$$V(x) = V_0 \left(\left(\left(\frac{x}{a} \right)^2 - 1 \right)^2 - 1 - 0.3 \left(\frac{x}{a} \right) \right), \quad (62)$$

where $V_0 = mw^2a^2/8$, $a = 0.5$, $m = 10$, $w = 2$. The location of local minimum is $x_{local} = -0.5$, while the location of global minimum is $x^* = 0.5$. Denote the ground state to be $|0\rangle = |\psi_g(x)\rangle$, and let the initial state $|\psi_0\rangle = |\psi_0(x)\rangle$ and ground state be symmetric about $x = 0$, i.e., $\psi_0(x) = \psi_g(-x)$, shown in Fig. 2.

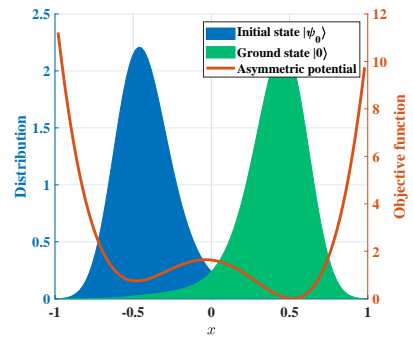


FIG. 2. Landscape of spontaneous emission: asymmetric potential (orange line), the distribution of initial state $|\psi_0\rangle$ (blue area), and the distribution of ground state $|0\rangle$ (green area).

The finite heat bath is simulated by numerically solving the Schrödinger equation using symplectic leapfrog scheme [50], where the Hamiltonian is given by Eq. (7). Since the simulation cost increases exponentially with respect to the number of oscillators, the energy level of oscillators is restricted to two, which means the Hamiltonian of the harmonic oscillator can be written as $H = \text{diag}(1/2, 3/2)\hbar\Omega$.

We first verify that the system can still reach the ground state with high probability, when there is only a single two-energy-level oscillator and the Hamiltonian of heat bath is $H_B = \text{diag}(1/2, 3/2)\hbar\Omega_1$. The parameter setting and results are shown in Fig. 3, which implicates that there exists a frequency $\Omega_1 = 0.905\Omega_0$ such that the system can reach the ground state with high probability $|\langle\psi(t)|0\rangle|^2 > 0.9$.

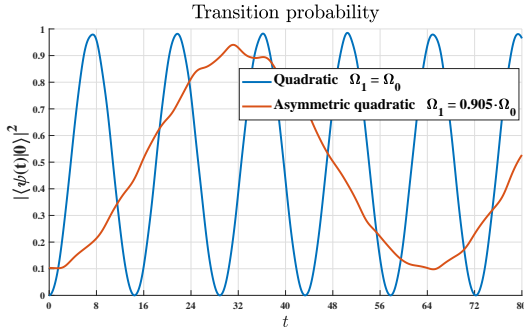


FIG. 3. Transition probability to the ground state, i.e., $|\langle\psi(t)|0\rangle|^2$. The quadratic case is a benchmark ($V(x) = \frac{1}{2}m\Omega_0^2x^2, \Omega_0 = w$), which exhibits characteristics of spontaneous emission (blue line). When $\Omega_1 = 0.905\Omega_0$, the system maximum probability of transition is larger than 0.9 (orange line).

We increase the number of oscillators in heat bath, where $n = 0, 5, 9, 11, 13$. The Hamiltonian of heat bath is $H_B = \sum_n \text{diag}(1/2, 3/2)\hbar\Omega_n$. For a physical system in the real world, the number of modes of frequency Ω_n should satisfy a specific distribution. For simplification, we choose the uniform distribution, namely the frequencies of oscillators being randomly chosen in the range $\Omega_n \in [0.7\Omega_0, 1.3\Omega_0]$. The results are shown in Fig. 4, which implicate that the probability of transition gradually stabilizes and stays in a high level with the increasing number of oscillators.

B. Implementation of numerical experiments for QLD

The simulation of QLD is achieved by numerically solving Eq. (16). We employ the implicit Euler method and an approximately uniform distribution $p(x)$ to ensure the stability of numerical computation. All parameters are configured in accordance with an actual physical system after nondimensionalization. Comprehensive details are provided in Appendix A 1.

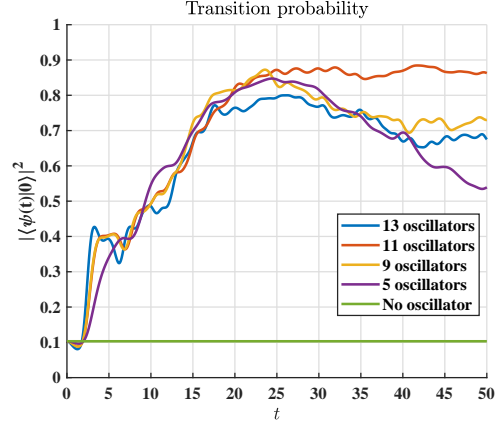


FIG. 4. Transition probability when increasing the number of harmonic oscillators in heat bath. Since the frequencies of oscillators are randomly chosen, the results of this experiment are not unique. We choose the best one to verify our statements.

C. Quadratic potentials

First, we verify whether the convergence values satisfy Eq. (53) and Eq. (54) by the following parameter setting [51].

Parameter Setting: Resolution $n = 128$, domain $x \in [-1, 1]$, space step $\Delta x = \frac{2}{n}$, time step $\Delta t = 0.05\Delta x^2$, total evolution time $t_f = 10$, $\hbar = 2.1108$, $kT = 165.8080$ ($T = 200$), characteristic damping rate $\eta = 5$, $\Omega = 223.2728$, $m = 1$, initial state $\psi_0(x) = \sqrt{p(x)}$. **Experiment Result:** The evolution of the probability distributions is shown in Fig. 5. The evolutions of the expectation values of Hamiltonian $\langle H \rangle_t$, potential energy $\langle V \rangle_t$ and kinetic energy $\langle E_k \rangle_t$ are shown in Fig. 6. The analytical solutions of convergence value $\langle V \rangle_f$ and $\langle E_k \rangle_f$ can be calculated by Eq. (53) and Eq. (54), which are $\langle V \rangle_f = 132.3762$, $\langle E_k \rangle_f = 132.4368$. Numerical experiments also give the convergence value $\langle V \rangle_f' = 132.1086$, $\langle E_k \rangle_f' = 132.6604$ with respect to density matrix at the final moment $t_f = 5$. As a result, numerical results are very close to theoretical results, while differences between them might be caused by numerical errors.

Then, we try to verify whether the system reaches the ground state at the low temperature regime, stated at the end of Section III B. The following parameter setting is used.

Parameter Setting: Resolution $n = 128$, domain $x \in [-1, 1]$, space step $\Delta x = \frac{2}{n}$, time step $\Delta t = 0.05\Delta x^2$, total evolution time $t_f = 10$, $\hbar = 2.1108$, $kT = 0.0083$ ($T = 0.01$), characteristic damping rate $\eta = 5$, $\Omega = 223.2728$, $m = 1$, initial state $\psi_0(x) = \sqrt{p(x)}$.

Experiment Result: The evolutions are shown in Fig. 7 and Fig. 8. Still using same notations as previous, we have $\langle V \rangle_f = 117.8211$, $\langle E_k \rangle_f = 117.8211$,

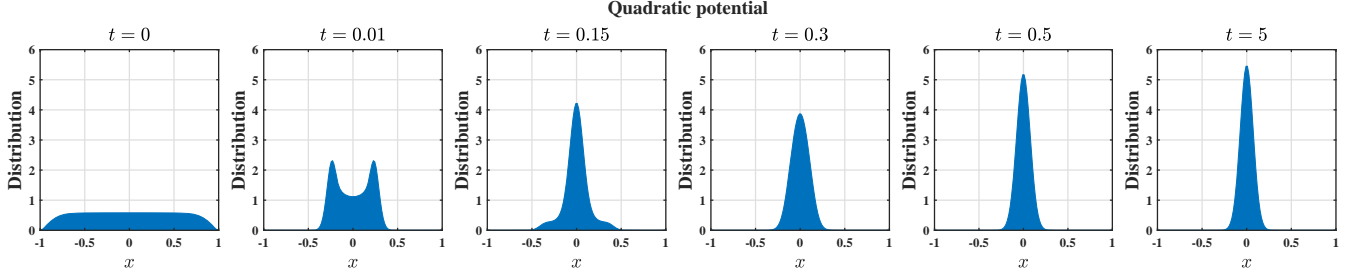


FIG. 5. The time evolution of probability distributions for quadratic potential at mild temperature. x-coordinate represents the position x , and y-coordinate represents the diagonal elements of density matrix. Six different moments $t = 0, 0.01, 0.15, 0.3, 0.5, 5$ with notable features are chosen. At the beginning of evolution, we can observe the oscillation of the probability distribution. After $t > 0.5$, the probability distribution converges to a stable distribution gradually because of dissipation.

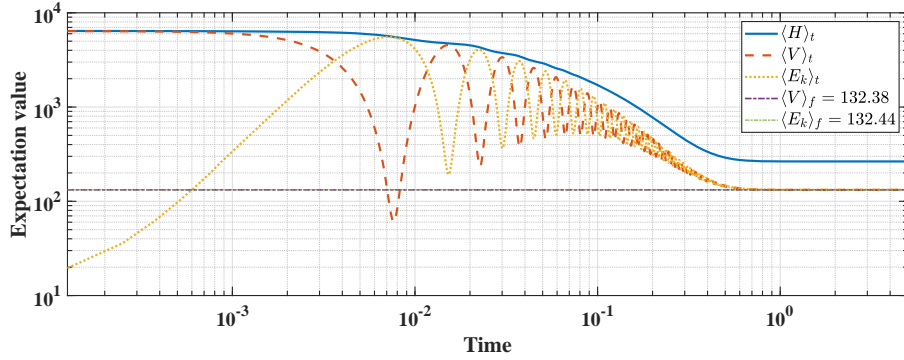


FIG. 6. The time evolution of expectation values for quadratic potential at mild temperature. x-coordinate represents the time t , and y-coordinate represents the expectation value of Hamiltonian $\langle H \rangle_t$, potential energy $\langle V \rangle_t$ and kinetic energy $\langle E_k \rangle_t$. The analytical convergence values $\langle V \rangle_f = 132.3762$, $\langle E_k \rangle_f = 132.4368$ are also shown in the figure as convergence lines. We can easily observe the oscillation of the expectation values at the beginning consistent with analytical solutions Eq. (49) and Eq. (52), which originates from $\cos(2\Omega t)$ and $\sin(2\Omega t)$ factors in these equations. During the whole process, the oscillation decays gradually, which results from the damping factor $\exp(-2\eta t)$.

$\langle V \rangle'_f = 117.4373$, $\langle E_k \rangle'_f = 117.8249$, analytical solution of ground state potential energy and kinetic energy is $\frac{1}{4}\hbar\Omega = 117.8211$. This consistency suggests that the system has reached the ground state. Denote ρ_f to be the numerical solution of density matrix at the final moment $t = 5$, and ρ_g to be the analytical solution of the ground-state density matrix. We use fidelity and quantum relative entropy to evaluate the closeness between the numerical result and analytical ground state, which derives fidelity $F(\rho_f, \rho_g) = \left(\text{Tr} \sqrt{\sqrt{\rho_f} \rho_g \sqrt{\rho_f}} \right)^2 = 0.9999902$ and quantum relative entropy (in Kullback-Leibler divergence) $D_{KL}(\rho_f \| \rho_g) = \text{Tr}(\rho_f (\ln(\rho_f) - \ln(\rho_g))) = 6.3466 \times 10^{-4}$, showing that the numerical result and analytical ground state are very close to each other.

D. Roles of each parameter

In this part, we discuss the role of each parameter in QLD separately. In Eq. (15), parameters η , $T(kT)$, Ω

play important roles in the behavior of the system. In order to analyze the roles of these parameters, we fix other parameters and change one of η , $T(kT)$, Ω each time.

In all experiments of this section, we use a double well potential because it can test the ability of QLD in escaping from the local minimum by quantum thermal effect and dissipative quantum tunneling effect while it keeps the simplicity of the potential. The double well potential is set in domain $x \in [-1, 1]$ as

$$V(x) = 83.9808x^4 - 64.8x^2 + 7.2x + 17.0680, \quad (63)$$

whose global minimum appears at $x^* = -0.6472$.

In order to evaluate the performance of algorithms, we introduce “success probability” [32] to measure the probability of finding the global minimum. The success probability is defined as the probability of finding the global minimum x^* within a certain tolerance $\epsilon = 0.15$, which is given by

$$\text{Pr}(\text{success}) = \text{Pr}(|x(t) - x^*| \leq \epsilon). \quad (64)$$

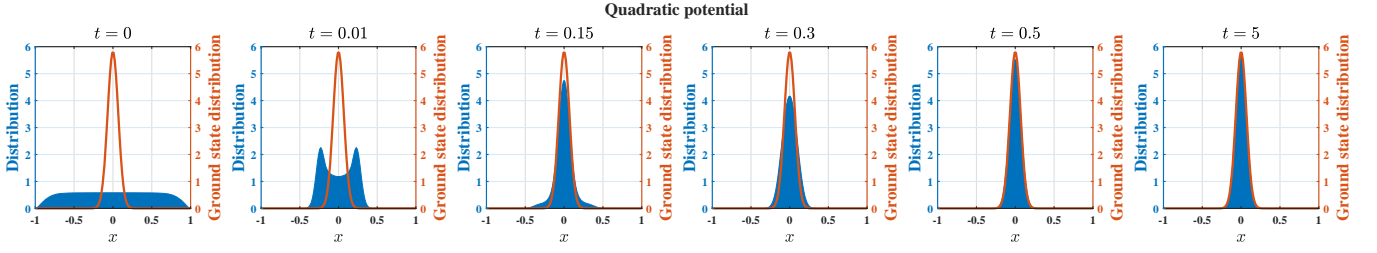


FIG. 7. The time evolution of probability distributions for quadratic potential at low temperature. x-coordinate represents the position x , and y-coordinate represents the diagonal elements of density matrix. Six different moments $t = 0, 0.01, 0.15, 0.3, 0.5, 5$ with notable features are chosen. The orange line is the analytical solution of ground state probability distribution. In the end, the system reaches the ground state.

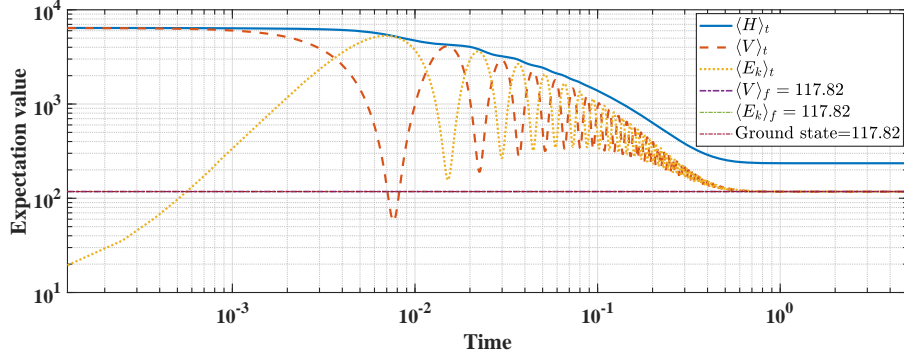


FIG. 8. The time evolution of expectation values for quadratic potential at low temperature. x-coordinate represents the time t , and y-coordinate represents the expectation value of Hamiltonian $\langle H \rangle_t$, potential energy $\langle V \rangle_t$ and kinetic energy $\langle E_k \rangle_t$. The analytical convergence values $\langle V \rangle_f = 117.8211$, $\langle E_k \rangle_f = 117.8211$ and $\frac{1}{4}\hbar\Omega = 117.8211$ are also shown in the figure as convergence lines. It could be observed that the system reaches ground state when $t = 5$.

The introduction of the concept “success probability” is necessitated by the presence of numerous objective functions with local minima near zero. Traditional loss functions struggle in these scenarios, failing to show the superiority of QLD.

1. Roles of characteristic damping rate η

No matter in quantum case or classical case, η influences the convergence speed of the system [9, 52]. η is related to the damping and dissipative effect in quantum Langevin system. When η increases, the system will reach the stationary distribution faster, and vice versa. We also guess that if η is too large, the system will reach the stationary solution so quickly that the system cannot escape from the local minimum, weakening the performance of QLD. This guess is also verified in our following experiments. In order to evaluate the role of η individually, we set appropriate temperature and \hbar , and then use different η to see the speed of convergence.

Parameter Setting: Use different damping rates $\eta = 0.5, 1, 2, 3, 5, 7, 10, 20, 30, 50, 100$, while other parameters are invariant. Resolution $n = 128$, domain $x \in [-1, 1]$, space step $\Delta x = \frac{2}{n}$, time step $\Delta t =$

$0.05\Delta x^2$, total evolution time $t_f = 10$, $\hbar = 2.1108$, $kT = 2072.6$ ($T = 2500$), $\Omega = 300$, $m = 1$, initial state $\psi_0(x) = \sqrt{p(x)}$.

Experiment Result: Fig. 9 shows the probability distributions of different η at final moment $t_f = 10$. Fig. 10 shows the evolution of expectation values. From Fig. 9 and Fig. 10, we can observe when η is too small, the system has not reached the stationary distribution at $t = 10$ still needing extra time to evolve. When η is too large, the system reaches the stationary distribution so fast that system cannot escape from local minimum completely and the convergence value of potential energy increases. Within a suitable range of $\eta \in [5, 30]$, η does not have a significant impact on the expectation value at $t = 10$. Nevertheless, we have to admit that all observations of η are only available at this double well potential with form Eq. (63), and changing the objective function may influence the behavior of η .

2. Roles of \hbar and T

The performance of QLD mainly depends on \hbar and T . We first consider the roles of them separately, and then combine them to find the best strategy for optimization.

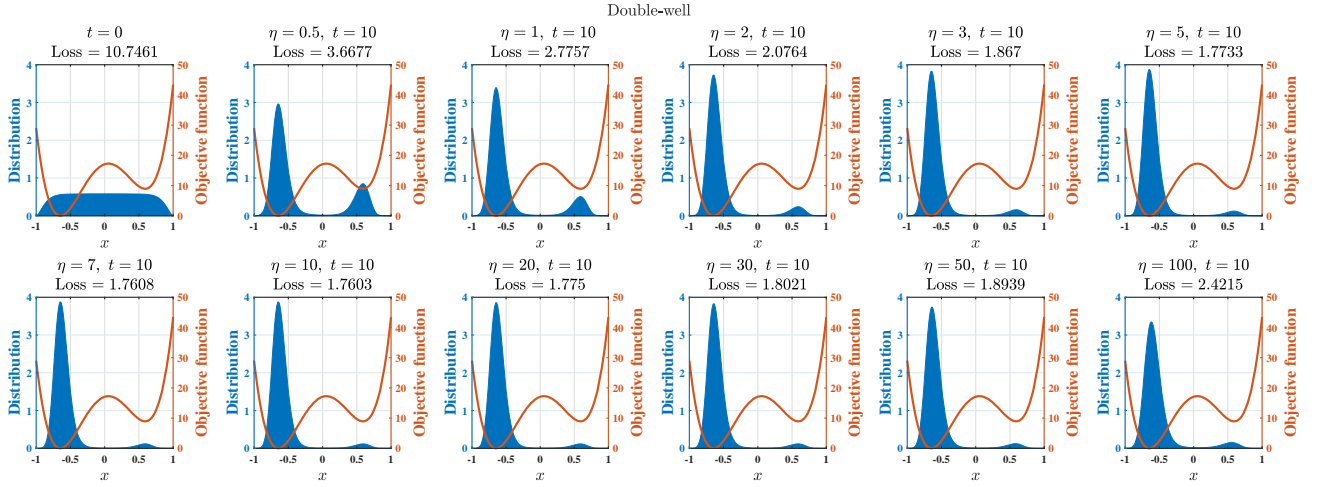


FIG. 9. The probability distributions with different η at final moment $t = 10$. x-coordinate represents the position x , and y-coordinate represents the diagonal elements of density matrix (blue area). Orange line is the double-well objective function. The first subplot shows the approximately uniform distribution at $t = 0$, and the following subplots are distributions at final moment $t = 10$ with different η . Losses at final moment are written in the subtitles of subplots. We can observe that η affects the evolution speed of QLD.

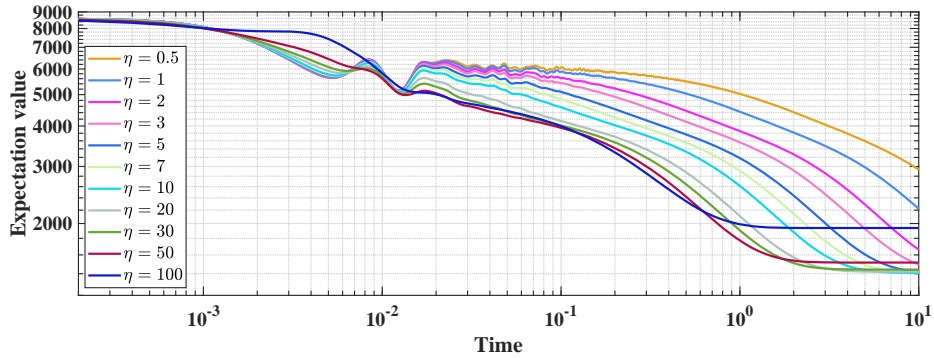


FIG. 10. The time evolution of expectation values of potential. x-coordinate represents the time t , and y-coordinate represents the expectation value. From this figure, we can observe when η is too small, the system has not reached the stationary distribution at $t = 10$ still needing extra time to evolve. When η is too large, the system reach the stationary distribution so fast that system cannot escape from local minimum completely and the convergence value of potential energy increases. Within a suitable range of $\eta \in [5, 30]$, η does not have a significant impact on the expectation value at $t = 10$.

\hbar is the unique parameter that only exists in the quantum case, which determines the quantum tunneling effect in QLD. There are plenty of previous results for dissipative quantum tunneling. The most famous one is Ref. [53] by Caldeira and Leggett, with subsequent works [54–60]. To study the tunneling effect, we need to turn off the thermal term, which means setting an extremely low temperature in the experiments. In order to show the power of quantum tunneling, the initial wave function ψ_0 is set near the local minimum $x_{local} \approx 0.6$, and it follows a Gaussian distribution:

$$\psi_0 = \frac{1}{\sqrt{2\pi\sigma^2}} \exp\left(-\frac{(x-x_1)^2}{2\sigma^2}\right), \quad x_1 = 0.6, \sigma = 0.08. \quad (65)$$

Parameter Setting: Change the reduced Planck constant $\hbar = 1, 2.1108, 4, 8, 12, 16, 20, 24, 28, 32, 36$, while other parameters are invariant in each case. Resolution $n = 128$, domain $x \in [-1, 1]$, space step $\Delta x = \frac{2}{n}$, time step $\Delta t = 0.05\Delta x^2$, total evolution time $t_f = 10$, $kT = 0.0083$ ($T = 0.01$), $\eta = 5$, $\Omega = 300$, $m = 1$, initial state: Gaussian distribution Eq. (65).

Experiment Result: The distributions with different \hbar at $t = 10$ are shown in the Fig. 11. We observe that the quantum tunneling effect is stronger when increasing the value of \hbar , but when \hbar is so large that it might cause significant fluctuation, making the system incapable of concentrating on the global minimum.

Temperature determines the thermal effect in QLD. As shown in the above experiments of \hbar , in the double

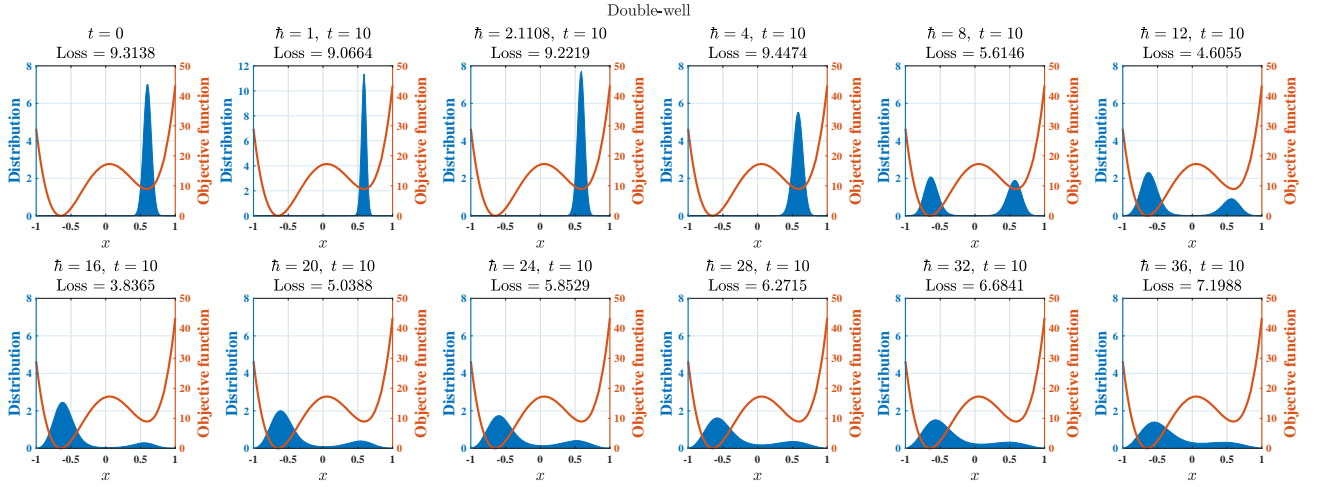


FIG. 11. The distributions with different \hbar at $t = 10$. x-coordinate represents the position x , and y-coordinate represents the diagonal elements of density matrix (blue area). The first subplot shows the initial distribution Eq. (65) at $t = 0$. Losses at final moment are written in the subtitles of subplots. We observe that quantum tunneling effect is stronger when increasing the value of \hbar , but when \hbar is so large that it might cause significant fluctuation which makes distribution not concentrate on the global minimum.

well landscape, the tunneling effect is negligible when $\hbar < 4$ (not applicable in all landscapes). In order to evaluate the roles of temperature T individually, we set $\hbar = 2.1108$.

Parameter Setting: Change the temperature $T = 50, 100, 200, 500, 800, 1000, 2000, 2500, 3500, 5000, 8000$ ($k = 0.82904$), while other parameters are invariant. Resolution $n = 128$, domain $x \in [-1, 1]$, space step $\Delta x = \frac{2}{n}$, time step $\Delta t = 0.05\Delta x^2$, total evolution time $t_f = 10$, $\hbar = 2.1108$, $\eta = 20$, $\Omega = 300$, $m = 1$, initial distribution: Gaussian distribution Eq. (65).

Experiment Result: The distributions with different T at final moment $t = 10$ are shown in the Fig. 12. We observe that the thermal effect is very subtle at the low temperature region, manifesting as the system being stuck at a local minimum and unable to escape, while at high temperature region, the thermal effect is significant, manifesting as the system being able to escape from the local minimum and reach the global minimum. However, if the T is too high (e.g., $T = 8000$), the thermal effect is so strong that the system is unable to concentrate on the minimum because of fluctuation.

When considering T and \hbar together, tunneling and thermal effect both exist. The performance and success probability of QLD not only depend on T and \hbar , but also its evolution time. We set a range of T and \hbar for $T \in [1000, 2800]$ and $\hbar \in [6, 24]$, then choose the double well landscape to discuss the combined effect.

Parameter Setting: Conduct 100 cases, where $T = 1000, 1200, 1400, 1600, 1800, 2000, 2200, 2400, 2600, 2800$ and $\hbar = 6, 8, 10, 12, 14, 16, 18, 20, 22, 24$ respectively, while $\eta = 20$ is fixed. We set an upper bound of the total evolution time $t_f \leq 100$, since it takes too long for some cases to reach the steady state. $\Omega = 300$, $m = 1$,

initial state $\psi_0(x) = \sqrt{p(x)}$. Establish the criterion of steady state: let the k -th iteration of success probability be $\text{Pr}^{(k)}$, defined by Eq. (64). Cease iteration when $|\text{Pr}^{(k)} - \text{Pr}^{(k-1)}| < 10^{-7}$.

Experiment Result: As shown in Fig. 13, we observe that there exists a best temperature when \hbar is fixed. Furthermore, although smaller \hbar leads to higher success probability, the evolution time increases dramatically with respect to the decrease of \hbar . Due to the constraints of evolutionary economics, we cannot set \hbar and T to be too small.

E. Comparison with classical dynamics

It is well known that the stochastic differential equation approximates the discrete-time SGD algorithm and the Fokker-Plank-Smoluchowski equation (FPE) can be derived from the lr-dependent SDE by Itô's formula [9]. In the overdamped classical Langevin dynamics, the classical probability distribution ρ of the particle evolves according to the Smoluchowski equation [34]:

$$\frac{\partial \rho}{\partial t} = -\frac{1}{\gamma} \nabla \cdot (\rho \nabla V) + \frac{kT}{\gamma} \nabla^2 \rho, \quad (66)$$

where γ is the friction coefficient that satisfies $\gamma = 2m\eta$. It is the counterpart of FPE derived from SDE.

We compare QLD with FPE. In some landscapes, classical algorithms have demonstrated efficacy, and the advantages of quantum algorithms are not manifested. Hence, we choose a landscape that poses a comparatively challenging task for classical algorithms to serve as a basis for comparison, shown in Fig. 14. This function is called

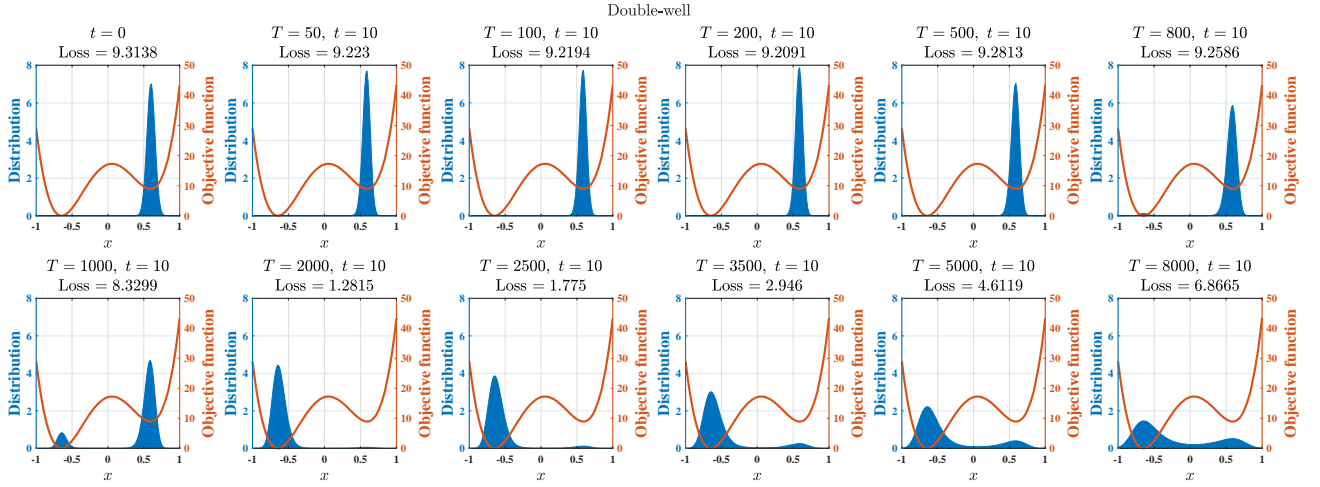


FIG. 12. The probability distributions with different temperature T at final moment $t = 10$. x -coordinate represents the position x , and y -coordinate represents the diagonal elements of density matrix (blue area). The first subplot shows the initial distribution Eq. (65) at $t = 0$. We observe that the thermal effect is very subtle at the low temperature region, manifesting as the system being stuck at a local minimum and unable to escape, while at high temperature region, the thermal effect is significant, manifesting as the system being able to escape from the local minimum and reach the global minimum. However, if the T is too high (e.g., $T = 8000$), the thermal effect is so strong that the system is unable to concentrate on the minimum because of fluctuation.

the Griewank function with form Eq. (A10), which is a nonconvex function with many local minima approximating zero.

Parameter Setting: We fix the temperature of QLD and FPE while changing \hbar of QLD. Parameters of QLD: Resolution $n = 128$, domain $x \in [-1, 1]$, $\Delta x = \frac{2}{n}$, time step $\Delta t = 0.5\Delta x^2$, $\Omega = 300$, $m = 1$. Change $T = 200, 1200, 2200$, $\hbar = 4, 10, 16$. Parameters of FPE: all the parameters are the same as QLD, except $\gamma = 2m\eta = 40$.

Experiment Result: As shown in Fig. 15, QLD and FPE exhibit entirely distinct characteristics. FPE performs better at high temperature, whereas QLD excels at low temperature. This observation aligns intuitively with classical dynamics, which necessitates higher temperatures for escaping local minima, consequently influencing the overall result quality. In contrast, QLD benefits from lower temperatures for effective energy dissipation, facilitating its transition to lower-energy subspace.

V. TIME-DEPENDENT QLD

Based on the conclusions drawn in Section IV E, QLD does not demonstrate a significant advantage in situations where classical algorithms already perform well. Conversely, in landscapes where classical algorithms exhibit shortcomings, QLD shows only marginal superiority. This implies that we have not fully leveraged the advantages inherent in quantum physics. Consequently, we propose a time-dependent QLD to address this limitation.

In this section, we extend Theorem 1 to accommodate time-dependent scenarios. Specifically, we allow the parameters η, \hbar, T in Eq. (15) to be time-dependent, denoted as $\eta(t), \hbar(t), T(t)$. Notably, the convergence of the time-dependent QLD is not only maintained but also exhibits improved performance in convex and slightly nonconvex cases, see Section V A for the details. By introducing the parameter $\eta(t)$, the convergence speed of QLD becomes $O(e^{-\int_0^t \eta(t') dt'})$. When carefully selecting an appropriate function $\eta(t)$, QLD can even achieve faster convergence. The time-dependent factors $\hbar(t)$ and $T(t)$ allow us to gradually decrease the strength of quantum tunneling and thermal fluctuation, respectively. This gradual decrease helps concentrate the optimization process towards the global minimum in the nonconvex case.

Section V B introduces process for selecting nonconvex objective functions. These functions are categorized into five groups, each with distinct features. In Section V C, we provide an example of a specific time-dependent QLD for the nonconvex case by specifying the functions $\hbar(t)$ and $T(t)$.

We compare QLD with other state-of-the-art algorithms, including Quantum Hamiltonian Descent (QHD) [32], Quantum Adiabatic Algorithm (QAA), Stochastic Gradient Descent (SGD) and Nesterov's accelerated gradient descent (NAGD) for different nonconvex objective functions, in Section V D and Section V E. The first three algorithms are quantum algorithms, and the last two are classical algorithms. All quantum algorithms are simulated on classical computers to visualize the evolution of probability distributions. Finally, we summarize the results of comparison and put forward a three-phase diagram to explain the superiority of QLD in the nonconvex

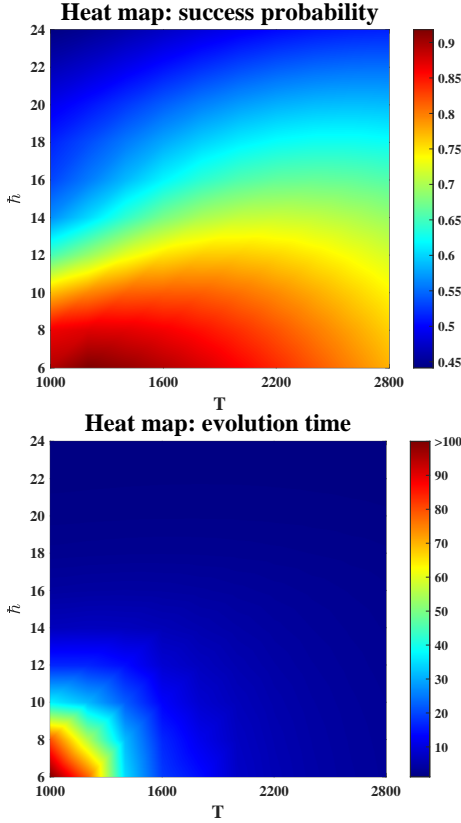


FIG. 13. We observe that there exists a best temperature when \hbar is fixed. Furthermore, although smaller \hbar leads to higher success probability, the evolution time increases dramatically with respect to the decrease of \hbar . Due to the constraints of evolutionary economics, we cannot set \hbar and T to be too small.

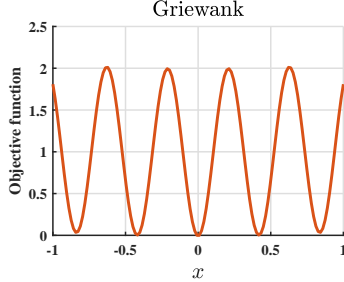


FIG. 14. Objective function: Griewank function $y = \frac{(15x)^2}{4000} - \cos(15x) + 1$. The global minimum appears at $x^* = 0$.

case, see Section V F.

A. Convergence of time-dependent QLD

In this section, we prove the convergence of time-dependent QLD in the convex case. We first evolve the time-dependent parameters $\eta(t)$, $\hbar(t)$, $T(t)$ to QLD respectively in Corollaries 1–3. Ultimately, we briefly discuss how to evolve them simultaneously.

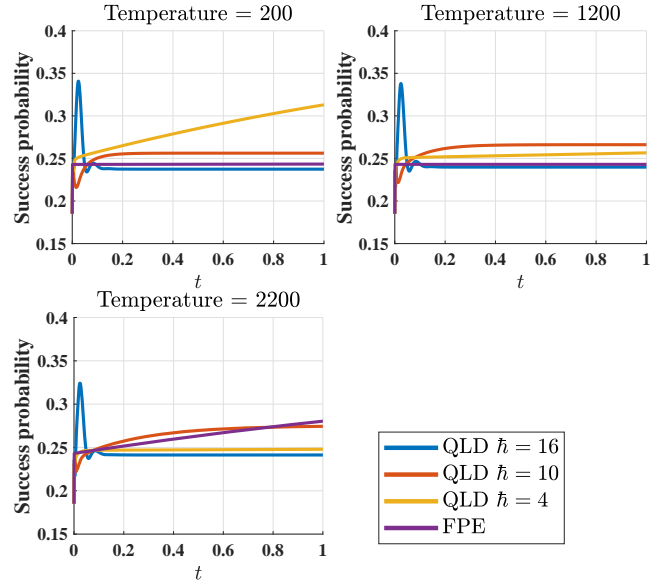


FIG. 15. Success probabilities of QLD (with different \hbar) and FPE at different temperatures. FPE demonstrates superior performance in high-temperature conditions, while QLD thrives in lower temperature environments.

1. Time-dependent $\eta(t)$

Note that the damping rate $\eta > 0$ in Theorem 1 is a constant during the evolution. We generalize $\eta = \eta(t) > 0$ for all $t \geq 0$, with the understanding that we can incrementally increase η to enhance the convergence speed of QLD, without compromising its effectiveness in escaping from local minima. Consequently, we can prove the following corollary of Theorem 1.

Corollary 1. *Only let η in Theorem 1 be a time-dependent parameter $\eta(t)$, and keep other parameters and requirements consistent with Theorem 1. In this case, Eq. (17) becomes*

$$\langle V \rangle_t - V(x^*) \leq 2kT + O(e^{-\int_0^t \eta(t') dt'}).$$

Proof. The validity of Lemma 1 holds even when $L_j = L_j(t)$. Consequently, Eq. (26) remains applicable when $\eta = \eta(t)$. This, in turn, establishes that Eq. (28b) also continues to hold. Under the approximation $\hbar\Omega \ll kT$, Eq. (34) becomes

$$\frac{d}{dt} \langle H \rangle_t \leq \eta(t) \cdot (2kT - \langle H \rangle_t), \quad (67)$$

in which the only difference is $\eta = \eta(t)$. Then, defining a function $h(t) = (\langle H \rangle_t - 2kT)e^{\int_0^t \eta(t') dt'}$, it can be directly verified that $\frac{dh(t)}{dt} \leq 0$ for $\forall t > 0$ by Eq. (67). Therefore, $h(t) \leq h(0)$, and

$$\begin{aligned} \langle H \rangle_t - 2kT &\leq (\langle H \rangle_0 - 2kT)e^{-\int_0^t \eta(t') dt'} \\ &= O(e^{-\int_0^t \eta(t') dt'}). \end{aligned} \quad (68)$$

Using Eq. (19), we get $\langle V \rangle_t \leq \langle H \rangle_t \leq 2kT + O(e^{-\int_0^t \eta(t') dt'})$. \square

By dynamically modulating the value of $\eta(t)$ at various stages of the evolution process, we can effectively control the convergence rate of the QLD, thereby enabling acceleration or deceleration of its convergence speed as needed.

2. Time-dependent $\hbar(t)$

In the numerical experiments of time-independent \hbar , we observe that larger \hbar can reinforce the effect of quantum tunneling to escape from local minimums, however, it also makes the system incapable of concentrating on the minimum. In order to solve this problem, we prove the following corollary of Theorem 1 with monotonically decreasing $\hbar(t)$ with respect to t .

Corollary 2. *Only let \hbar in Theorem 1 be a time-dependent parameter $\hbar(t)$, which satisfies $\frac{d\hbar(t)}{dt} \leq 0$ and $\hbar(t) > 0$ for $\forall t \geq 0$, while still keeping other parameters and requirements consistent with Theorem 1. In this case, Eq. (17) still holds*

$$\langle V \rangle_t - V(x^*) \leq 2kT + O(e^{-\eta t}).$$

Proof. The validity of Lemma 1 holds even when $\hbar = \hbar(t)$. Then the first term on the right-hand side of Eq. (26) is non-zero now, becoming

$$\left\langle \frac{d}{dt} H \right\rangle_t = \left\langle \frac{d}{dt} \left(\frac{p^2}{2m} + V \right) \right\rangle_t = \left\langle \frac{p}{m} \frac{dp}{dt} \right\rangle_t. \quad (69)$$

Using $p = -i\hbar(t)\nabla$, we get

$$\frac{dp}{dt} = -i \frac{d\hbar}{dt} \nabla = \frac{p}{\hbar} \frac{d\hbar}{dt} = p \frac{d \ln \hbar}{dt}. \quad (70)$$

Inserting the above equation into Eq. (69), Eq. (69) becomes

$$\left\langle \frac{d}{dt} H \right\rangle_t = \left\langle \frac{p^2}{m} \frac{d \ln \hbar}{dt} \right\rangle_t = \frac{d \ln \hbar}{dt} \cdot \left\langle \frac{p^2}{m} \right\rangle_t. \quad (71)$$

At the same time, it is not difficult to verify that the second term and the third term on the right-hand side of Eq. (26) are still same here. Therefore, Eq. (28b) becomes

$$\begin{aligned} \frac{d}{dt} \langle H \rangle_t &= \frac{d \ln \hbar}{dt} \cdot \langle p^2/m \rangle_t + \left(\frac{\hbar^2 \mu^2}{m} + \frac{\eta^2}{4\mu^2} \langle \nabla^2 V \rangle_t \right) \\ &\quad - \eta \langle x \cdot \nabla V + p^2/m \rangle_t. \end{aligned} \quad (72)$$

Under the approximation $\hbar(t)\Omega \ll kT$, Eq. (33) becomes

$$\begin{aligned} \frac{d}{dt} \langle H \rangle_t &\leq \frac{d \ln \hbar}{dt} \cdot \langle p^2/m \rangle_t \\ &\quad + \eta \cdot (2kT - \langle V + p^2/(2m) \rangle_t). \end{aligned} \quad (73)$$

Because $\frac{d\hbar(t)}{dt} < 0$, we get $\frac{d \ln \hbar(t)}{dt} < 0$, and $\langle p^2/m \rangle_t \geq 0$, inducing the following inequality

$$\frac{d}{dt} \langle H \rangle_t \leq \eta \cdot (2kT - \langle V + p^2/(2m) \rangle_t), \quad (74)$$

which is the same as Eq. (34). Then, the rest of the proof is similar to that of Theorem 1 and Proposition 2. \square

3. Time-dependent $T(t)$

We also investigate the impact of a time-dependent temperature, $T(t) > 0$, on the convergence of QLD. Given that $2kT$ influences the precision of QLD (refer to Remark 1), possessing a progressively diminishing $2kT$ can enhance the precision of QLD. Additionally, it can intensify the thermal effect to escape from the local minimum when T is initially high at the onset of the evolution process. Under the aforementioned perspective, we have the following corollary of Theorem 1.

Corollary 3. *There exists a function f in relation to $T(\cdot)$, with properties:*

1. $\lim_{T \rightarrow 0^+} f(T) = 0^+$,
2. $f(T) \geq T$ for $\forall T > 0$,
3. $df(T)/dT > 0$ for $\forall T > 0$.

There also exists another function $G(\cdot)$ which depends on f and is a monotonically decreasing function. If temperature T is a time-dependent parameter $T(t)$ which satisfies $dT/dt \leq 0$ and $T(t) \leq G(t)$ for $\forall t \geq 0$, Eq. (17) becomes

$$\langle V \rangle_t - V(x^*) \leq 2kf(T(t)) + O(e^{-\eta t}),$$

if we still keep other parameters and requirements consistent with Theorem 1.

Proof. Similar to the proof of Corollary 1, we can find that Eq. (34) holds here:

$$\frac{d}{dt} \langle H \rangle_t + \eta \cdot (\langle H \rangle_t - 2kT(t)) \leq 0. \quad (75)$$

Defining a function $h(t) = (\langle H \rangle_t - 2kf(T(t)))e^{\eta t}$, its time derivative can be calculated as

$$\begin{aligned} \frac{dh(t)}{dt} &= \left(\frac{d}{dt} \langle H \rangle_t - 2k \frac{df}{dT} \frac{dT}{dt} \right) e^{\eta t} \\ &\quad + (\langle H \rangle_t - 2kf(T(t))) \eta e^{\eta t}. \end{aligned} \quad (76)$$

If there exists functions $f(T)$ and $T(t)$ that satisfy (we will prove their existence later)

$$\frac{df}{dT} \frac{dT}{dt} + \eta f(T) \geq \eta T > 0, \quad (77)$$

it is direct to verify that

$$\left(\frac{d}{dt} \langle H \rangle_t - 2k \frac{df}{dT} \frac{dT}{dt} \right) + \eta (\langle H \rangle_t - 2kf(T(t))) \quad (78)$$

$$\leq \frac{d}{dt} \langle H \rangle_t + \eta \cdot (\langle H \rangle_t - 2kT(t)) \leq 0, \quad (79)$$

in which the second inequality comes from Eq. (75). Multiplying $e^{\eta t}$ on Eq. (78), we get

$$\frac{dh(t)}{dt} \leq 0. \quad (80)$$

Then $h(t) \leq h(0)$ implies $\langle H \rangle_t - 2kf(T(t)) \leq O(e^{-\eta t})$. Using Eq. (19), we get $\langle V \rangle_t \leq \langle H \rangle_t \leq 2kf(T(t)) + O(e^{-\eta t})$.

Therefore, we only need to prove the existence of functions $f(T)$ and $T(t) \leq G(t)$ satisfying all the properties in this corollary.

Define $f(T) = T_c(e^{T/T_c} - 1)$, which satisfies all properties of $f(\cdot)$ in this corollary, where T_c is any constant temperature to ensure dimensional consistency. Inserting $f(T) = T_c(e^{T/T_c} - 1)$ into Eq. (77), we get

$$e^{T/T_c} \frac{dT}{dt} + \eta T_c(e^{T/T_c} - 1) \geq \eta T, \quad (81)$$

which can be rewritten as

$$0 \geq \frac{dT}{dt} \geq \eta \frac{T - T_c(e^{T/T_c} - 1)}{e^{T/T_c}}. \quad (82)$$

Here, we mainly focus on $\frac{dT}{dt} \leq 0$ consistent with the corollary, because Eq. (81) is obviously true when $\frac{dT}{dt} > 0$. Eq. (82) can be transformed into (consider $dt > 0, dT \leq 0$)

$$0 \leq \frac{e^{T/T_c}}{T - T_c(e^{T/T_c} - 1)} dT \leq \eta dt. \quad (83)$$

Integrate both sides of the above equation

$$\int_{T(0)}^{T(t)} \frac{e^{T/T_c}}{T - T_c(e^{T/T_c} - 1)} dT \leq \eta \int_0^t dt' = \eta t, \quad (84)$$

where $T(t) \leq T(0)$ for $t > 0$. Denote the integration $\int \frac{e^{T/T_c}}{T - T_c(e^{T/T_c} - 1)} dT = \mathcal{G}(T)$ [61]. Obviously, $\mathcal{G}(T)$ is a monotonically decreasing function with respect to T . As a result, we have

$$\mathcal{G}(T(t)) - \mathcal{G}(T(0)) \leq \eta t, \quad (85)$$

which implies

$$T(t) \leq \mathcal{G}^{-1}(\eta t + \mathcal{G}(T(0))). \quad (86)$$

Set $G(t) = \mathcal{G}^{-1}(\eta t + \mathcal{G}(T(0)))$, we obtain the function $G(t)$ stated in this corollary. \square

Remark 3. It is not difficult to verify that when $T(t)$ is a constant and $f(T) = T$, Corollary 3 is reduced to Theorem 1.

Remark 4. By this corollary, we can actualize Remark 1 by judiciously selecting a $T(t)$ such that $f(T(t))$ is minimized to the desired precision level ε .

4. Three time-dependent parameters $\eta(t), \hbar(t), T(t)$

Finally, we consider the case where all three parameters $\eta(t), \hbar(t), T(t)$ are time-dependent. If Corollaries 1–3 are satisfied simultaneously, then we have

$$\langle V \rangle_t - V(x^*) \leq 2kf(T(t)) + O(e^{-\int_0^t \eta(t') dt'}), \quad (87)$$

whose proof, similar to the proof of Corollaries 1–3, is omitted here.

B. Objective functions

In this part, we succinctly introduce the objective functions used in our nonconvex function experiments. Many objective functions of global optimization are multidimensional [32, 62–66]. However, we can only conduct one-dimensional experiments on classical computers due to the computational cost (each one-dimensional QLD experiment requires approximately 14 hours). Consequently, we transform several multidimensional objective functions into one-dimensional ones, ensuring the preservation of their most significant characteristics within the landscapes. Finally, 7 nonconvex functions are split into 5 different categories by the characteristics of their landscapes [32]. Each of them only has one global minimum $x^* = 0$. By shifting the functions vertically, we set the global minimum value $V(x^*) = 0$.

Ref. [32] also explains how to categorize different objective functions. The category “Ridges or Valleys” is featured by small deep sections that divide the domain. “Basin” is featured by flatness near the global minimum of function values. “Flat” is featured by its flatness at elevated function values. “Studded” is identified by a foundational shape that exhibits high-frequency perturbations. The category “Simple” represents functions that can be solved efficiently by standard gradient descent algorithms. The functions in each category are listed in Table I, whose precise formulations can be found in Appendix A 2.

TABLE I. Test functions classification.

Features	Function names
Ridges or Valleys	Deflected Corrugated Spring (DCS)
Basin	Csendes
Flat	Michalewicz
Studded	Alpine 1, Bohachevsky 2, Griewank
Simple	Double well

C. Time-dependent Quantum Langevin Dynamics

In the previous experiments, we analyze roles of T, η, \hbar in QLD, which also lead to the question why QLD would

have a better performance if these parameters are time-dependent, as different ranges of parameters have different effect in different phases of the optimization process. At the beginning of the evolution, we set a high temperature to prompt the system to escape from local minimum. Then, we reduce the temperature to cool the system, allowing it to reach a more optimal, lower energy state. The discussion concerning \hbar is also similar. At the beginning of the evolution, larger \hbar can accelerate the rate of quantum tunneling, helping system escape from local minimum. After seeking the global minimum, smaller \hbar , weakening the quantum tunneling effect, can prevent system from tunneling back to local minimum. If \hbar and T decrease at the same time, \hbar must decrease faster than T as the effect of tunneling back to local minimum is very significant at a mild temperature, termed as “quantum anti-tunneling”. This could be due to the large value of \hbar , which violates the approximation $\hbar\Omega \ll kT$ as stated in Corollaries 1–3. This violation could trigger the “quantum anti-tunneling” phenomenon. Therefore, $\hbar(t)$ needs to decrease faster than $T(t)$ as Eq. (89) and Eq. (90). This might ensure that the system can concentrate on the global minimum after escaping from local minimum.

From the above analysis, we decide to use inverted Sigmoid function to establish time-dependent $\hbar(t)$ and $T(t)$, which is also well known as the (inverted) Richards curve [67]. The inverted Sigmoid function $Y(t)$ is defined as

$$Y(t) = Y_l + \frac{Y_u - Y_l}{1 + \exp(\tilde{k}(t - \tau))}, \quad (88)$$

where Y_l and Y_u are the lower and upper bounds, respectively, \tilde{k} is the growth (decline) rate, and τ is the time of maximum growth (decline).

In all experiments of time-dependent QLD, $\hbar(t)$ is set to be

$$\hbar(t) = 0.5 + \frac{25 - 0.5}{1 + \exp(1.2 \cdot (t - 0.4 \cdot t_f))}, \quad (89)$$

and $T(t)$ is set to be

$$T(t) = 2 + \frac{3000 - 2}{1 + \exp(1.2 \cdot (t - 0.52 \cdot t_f))}, \quad (90)$$

where t_f is the total evolution time. The curves of $\hbar(t)$ and $T(t)$ are shown in Fig. 16.

Same finite difference method and implicit Euler method as Section IVB are used to numerically solve the evolution of system. The only difference is that time-dependent $\hbar(t)$ and $T(t)$ make $\hat{\mathcal{L}}$ of Eq. (A1) be a time-dependent matrix $\hat{\mathcal{L}}(t)$. Dirichlet boundary condition and approximately uniform distribution are still kept here.

Parameter Setting: Resolution $n = 128$, domain $x \in [-1, 1]$, space step $\Delta x = \frac{2}{n}$, time step $\Delta t = 0.05\Delta x^2$, total evolution time $t_f = 10$, $\hbar(t)$ and $T(t)$ are Eq. (89) and Eq. (90), characteristic damping rate $\eta = 10$, $\Omega = 300$, $m = 1$, initial state $\psi_0(x) = \sqrt{p(x)}$.

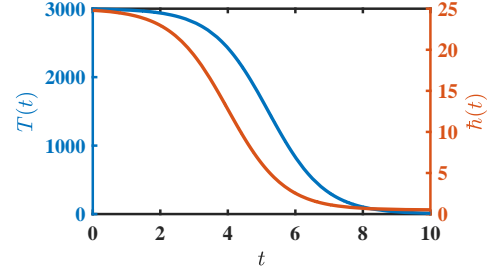


FIG. 16. Time-dependent $\hbar(t)$ and $T(t)$ for $t_f = 10$.

D. Quantum algorithms

We introduce another two quantum algorithms: Quantum Hamiltonian Descent (QHD) and Quantum Adiabatic Algorithm (QAA) as competitors of QLD.

1. Quantum Hamiltonian Descent (QHD)

We mainly follow Ref. [32] to implement QHD. The Hamiltonian of QHD is given by

$$H(t) = \left(\frac{2}{s_1 + t^3} \right) \left(-\frac{1}{2} \nabla^2 \right) + 2(s_2 + t^3) V(x). \quad (91)$$

In the ideal case, $s_1 = s_2 = 0$ [68]. We would like to note here that the damping parameter $\frac{1}{t^3}$ is just one possible choice, made for the purpose of comparing QHD with the classical Nesterov’s accelerated gradient descent algorithm directly. It is possible for QHD to achieve better performance with alternative damping parameter.

Then, we discretize the space into grids similar to Section IVB and use symplectic leapfrog scheme [50] to evolve this Hamiltonian system.

Parameter Setting: Resolution $n = 128$, domain $x \in [-1, 1]$, space step $\Delta x = \frac{2}{n}$, time step $\Delta t = 0.05\Delta x^2$, total evolution time $t_f = 10$, $s_1 = s_2 = 0.01$, initial state being the uniform distribution.

2. Quantum Adiabatic Algorithm (QAA)

Quantum Adiabatic Algorithm [69] is a famous quantum computing algorithm that takes advantage of the quantum adiabatic theorem to solve general optimization problems. Suppose the Hamiltonian changes gradually from initial H_i to final H_f , quantum adiabatic theorem states that if the system is initially in the n -th eigenstate of H_i , it will remain in the n -th eigenstate of H_f at final time t_f if the evolution is slow enough [70]. To be more precise, it follows the Schrödinger equation

$$i \frac{\partial \psi}{\partial t} = [(1 - g(t))H_i + g(t)H_f] \psi(t). \quad (92)$$

where $g(t)$ is a time-dependent function that satisfies $g(0) = 0$ and $g(t_f) = 1$. In order to solve optimization problems, we set H_f to be the problem Hamiltonian that encodes the problem of interest. The final state of the system represents the solution to the optimization problem. By measuring the final state, we can obtain the solution to the problem. Following Refs. [32, 71, 72], we adopt Radix-2 representation to solve continuous optimization problems. The initial Hamiltonian H_i is given by sum of Pauli- X operators

$$H_i = - \sum_{j=1}^N X_j, \quad (93)$$

whose ground state is the uniform superposition of all basis states. The final Hamiltonian H_f is given by diagonal matrix $V = \text{diag}(V(x_1), \dots, V(x_{2^N}))$.

The evolution of Eq. (92) is calculated numerically by symplectic leapfrog scheme [50].

Parameter Setting: Resolution $n = 2^N = 128$, domain $x \in [-1, 1]$, space step $\Delta x = \frac{2}{n}$, time step $\Delta t = 0.05 \Delta x^2$, total evolution time $t_f = 10$, $g(t) = \frac{t}{t_f}$, initial state being the uniform distribution.

E. Classical algorithms

This part describes Stochastic Gradient Descent (SGD) which is the classical counterpart of QLD, and another prestigious Nesterov's accelerated gradient descent (NAGD). Both of them are as competitors of QLD.

1. Stochastic Gradient Descent (SGD)

Stochastic Gradient Descent is widely used in machine learning and deep learning for training models to minimize the loss function [9]. Starting from an initial point x_0 , SGD updates the point by

$$x_{k+1} = x_k - s \nabla f(x_k) - s \xi_k, \quad (94)$$

where s is the step size (learning rate), ξ_k is a noise term at k -th iteration. The effective evolution time at the k -th step is $t_k = sk$. In our experiments, we set ξ_k to be a Gaussian random noise with zero mean and non-zero variance [32].

Parameter Setting: Domain $x \in [-1, 1]$, learning rate $s = 0.05 \cdot (\frac{2}{128})^2$, total evolution time $t_f = 10$, variance of Gaussian random noise $\sigma = 1$, 20000 initial points x_0 are uniformly randomly distributed on $[-1, 1]$.

2. Nesterov's accelerated gradient descent (NAGD)

Nesterov's accelerated gradient descent [73] is the classical counterpart of QHD, which iterates according to

$$\begin{aligned} x_k &= y_{k-1} - s \nabla f(y_{k-1}), \\ y_k &= x_k + \frac{k-1}{k+2} (x_k - x_{k-1}), \end{aligned} \quad (95)$$

where s is the step size. The initial points are chosen as $x_0 = y_0$. In some cases, it will converge faster than the standard gradient descent. The effective evolution time at the k -th step is $t_k = sk$ [32].

Parameter Setting: Domain $x \in [-1, 1]$, learning rate $s = 0.05 \cdot (\frac{2}{128})^2$, total evolution time $t_f = 10$, 20000 initial points $x_0 = y_0$ are uniformly randomly distributed on $[-1, 1]$.

F. Results of the comparison

In above experiments, we fix the domain of x to $[-1, 1]$ and all algorithms share the same total evolution time $t_f = 10$ and same time step Δt , $s = 0.05 \cdot (\frac{2}{128})^2$. Besides, all quantum algorithms share same resolution $n = 128$. Seven objective functions in Table I with different features are tested for each algorithm.

Here, we first show the results of Michalewicz function in Fig. 17 and Fig. 18, while the results of other objective functions are shown in Appendix A 3 due to space constraints. In these numerical experiments, we demonstrate that time-dependent QLD leads to superior performance in many landscapes.

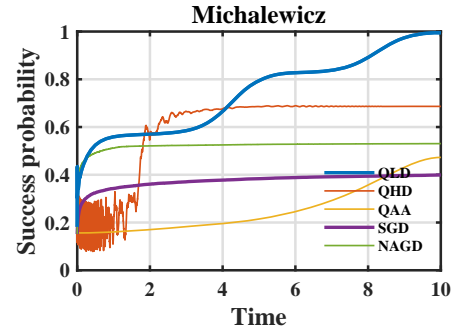


FIG. 17. Success probabilities of Michalewicz function for different algorithms at different (effective) evolution times.

Finally, based on the observations from Fig. 17, Fig. 18, and Appendix A 3, we categorize the entire evolution process into three distinct phases. This classification not only provides a comprehensive interpretation but also parallels the three phases of QHD [32]. In essence, we identify three key phases in the QLD evolution: the **thermal** phase, the **cooling** phase, and the **descent** phase.

Thermal phase. We set a high temperature and a large \hbar at first to leverage its tunneling and thermal capability. At this stage, the wave function rapidly narrows

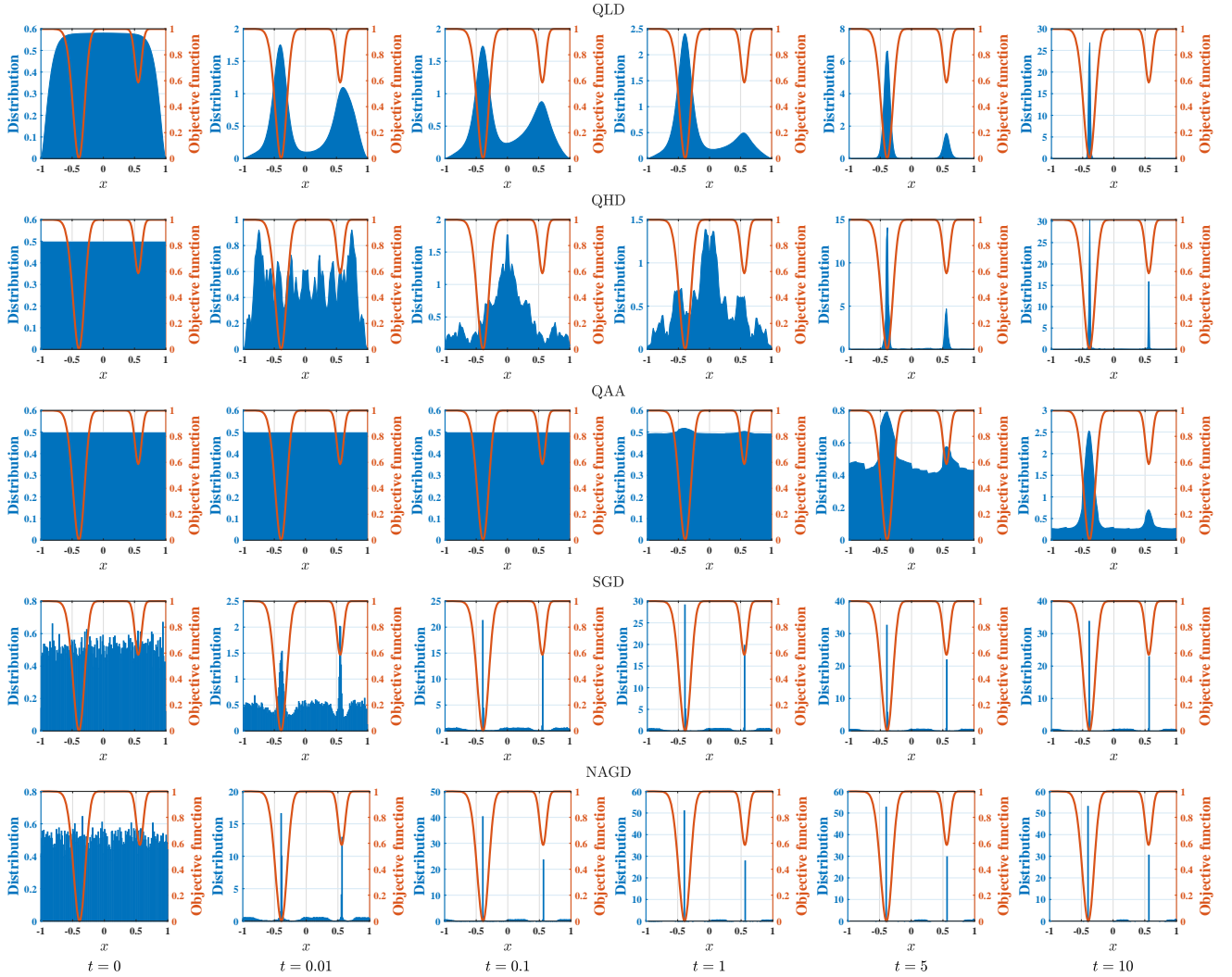


FIG. 18. Probability distributions of Michalewicz function ($x^* = -0.3911$) for different algorithms at different (effective) evolution times $t = 0, 0.01, 0.1, 1, 5, 10$.

the search domain. It serves as the global search phase in QHD [32].

Cooling phase. We extract energy from the heat bath and weaken the quantum tunneling effect artificially (low down the temperature and \hbar), to prepare our algorithm for concentrating to the global minimum in the low-energy subspace.

Descent phase. In the last phase, both the thermal and tunneling effect are insignificant. The wave function becomes more concentrated in a slow convergence rate.

VI. DISCUSSION AND CONCLUSIONS

In conclusion, we demonstrate the possibility of solving continuous optimization problems through the application of a specific class of open dissipative quantum dynamics. We have theoretical guarantee of the convergence of QLD; meanwhile, we verify our intuition and

provide a feasible cooling strategy through numerical experiments. In particular, although in some landscapes other algorithms have already performed well, by controlling the parameters of QLD, it can outperform all other algorithms in some other landscapes.

From a high-level perspective, this work can be seen as an attempt to construct optimization algorithms inspired by quantum physical systems (open quantum systems), which includes guiding the configuration of parameters based on their inherent physical significance. Through this approach, it is possible to maximally leverage the advantages offered by quantum mechanics in the process of addressing optimization problems.

However, there are several issues that necessitate further investigation. Theoretically, we believe that both the advantages and shortcomings of QLD can be interpreted more thoroughly. In particular, due to the complex formula of the quantum Langevin dynamics, we only provide the convergence of QLD under the approxima-

tions of $\hbar\Omega \ll kT$ and $T \rightarrow 0$. Since the limit $\hbar \rightarrow 0$ clearly gives a transition to the classical Langevin equation, where all commutators vanish in this limit, in a sense, we might just prove the convergence of QLD in the classical limit, and use its quantum effect in the process of convergence. Whether the convergence still exists without these approximations remains further discussion with more meticulous mathematical and physical analysis. Numerically, since the simulation in the one-dimensional landscape alone has consumed a considerable amount of our computational resources, numerical experiments in high dimension requires more efficient numerical methods and more powerful classical computers. This also demonstrates the necessity of analog (or digital) quantum computers.

ACKNOWLEDGMENTS

We thank Jiaqi Leng, Hao Wu, Shuohan Zhang, and Zhennan Zhou for helpful discussions. Z. C. and Y. L. acknowledge research funding from Tsien Excellence in Engineering Program of Tsinghua University and Tsinghua University Initiative Scientific Research Program. T. L. was supported by the National Natural Science Foundation of China (Grant Numbers 62372006 and 92365117), and a startup fund from Peking University.

Appendix A: Numerical results of different objective functions

In this appendix, we elucidate the specifics of numerical implementation in Appendix A 1, articulate the exact forms of all objective functions in Appendix A 2, and analyze numerical results of all algorithms across different objective functions in Appendix A 3.

1. Implementation details of numerical experiments for QLD

QLD is simulated by numerically solving Eq. (16). At first, we discretize each axis of domain into n grids [74] and use central difference scheme in space, such that all operators in the Eq. (16) can be approximated by matrices, making Eq. (16) become

$$\frac{\partial \hat{\rho}}{\partial t} = \hat{\mathcal{L}}\hat{\rho}, \quad (\text{A1})$$

where $\hat{\rho}(t)$ is column vector of length $n^2 \times 1$ transformed from $\rho(x, y, t)$, $\hat{\mathcal{L}}$ is an $n^2 \times n^2$ matrix representing the sum of all operators in central difference scheme. In order to overcome the instability of numerical calculation, we employ the implicit Euler method (backward Euler method) in the time scheme, which is given by

$$\hat{\rho}(t + \Delta t) = \left(I - \Delta t \hat{\mathcal{L}} \right)^{-1} \hat{\rho}(t), \quad (\text{A2})$$

where Δt is time step. Although implicit method costs a lot in computational time, it is more stable than explicit method.

Because objective function reaches positive infinity at the boundary of domain in most cases, it is reasonable to use Dirichlet boundary condition in our numerical experiments. However, other efforts are still needed to avoid the instability of numerical calculation. In order to maintain the stability at the boundary, we set initial probability distribution to be an approximately uniform distribution with form

$$p(x) = (-0.4742x^{10} - 0.0063x^2 + 0.4903)^2 / Z_p, \quad (\text{A3})$$

where Z_p is the normalization factor. (See Fig. 19.) It is a good approximation of the uniform distribution in the interval $[-1, 1]$ and also approximates zero at the boundary to achieve the numerical stability. In the following

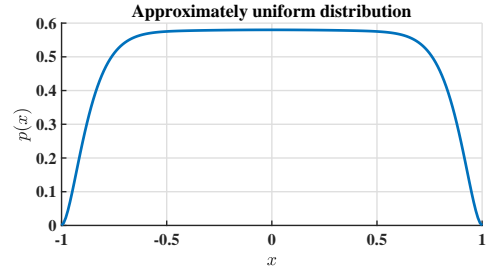


FIG. 19. The approximately uniform distribution in the interval $[-1, 1]$.

part, we will use this approximately uniform distribution to initialize our wave function $\psi_0(x)$ at time $t = 0$, which is given by

$$\psi_0(x) = \sqrt{p(x)}. \quad (\text{A4})$$

We also establish the time step size $\Delta t = 0.05\Delta x^2$, which is small compared to the width of the discretization grid Δx to ensure the stability of the numerical computation. In all numerical experiments, the domain of x is $[-1, 1]$. We only consider the one-dimensional case because each one-dimensional QLD experiment requires approximately 14 hours.

Nonetheless, a crucial challenge persists: determining the values of each parameter in Eq. (16). The system's behavior is highly sensitive to the quantities chosen for all parameters in Eq. (16). Refs. [41, 52, 75] study the dynamics of vibrational relaxation of a Morse oscillator, mimic the $\text{O}_2\text{-Pt}(111)$ bond, induced by equilibrium electrons. We have nondimensionalized this real physical system to obtain the baseline values for all parameters.

2. The precise formulations of objective functions

We choose seven objective functions with different features in Table I to test the performance of different algo-

rithms, as discussed in Section VB. The precise formulations and global minimums x^* of these objective functions defined in $x \in [-1, 1]$ are listed below,

- Deflected Corrugated Spring ($x^* = 0$):

$$V(x) = 0.1((6.5x)^2 + 25) - \cos\left(5\sqrt{(6.5x)^2 + 25}\right). \quad (\text{A5})$$

- Csendes ($x^* = 0$):

$$V(x) = x^6(2 + \sin(1/x)). \quad (\text{A6})$$

- Michalewicz ($x^* = -0.3911$):

$$V(x) = -\sin(1.2(x + 1.7)) \sin^2\left(\frac{2(1.2(x + 1.7))^2}{\pi}\right)^{20}. \quad (\text{A7})$$

- Alpine 1 ($x^* = 0$):

$$V(x) = |8x \sin(8x) + 0.8x|. \quad (\text{A8})$$

- Bohachevsky 2 ($x^* = 0$):

$$V(x) = 9x^2 - 0.3 \cos(9\pi x) + 0.3. \quad (\text{A9})$$

- Griewank ($x^* = 0$):

$$V(x) = \frac{1}{4000}(15x)^2 - \cos(15x) + 1. \quad (\text{A10})$$

- Double well ($x^* = -0.6472$):

$$V(x) = 83.9808x^4 - 64.8x^2 + 7.2x + 17.0680. \quad (\text{A11})$$

3. Analysis of numerical results

The results of Michalewicz function are shown in Section VF. Due to space constraints, the numerical results of rest six objective functions are shown here. The success probabilities of six objective functions for different algorithms at different (effective) evolution times are shown in Fig. 20. The probability distributions of six objective functions for different algorithms at different (effective) evolution times are shown in Figs. 21–26.

Based on the observations of Fig. 20, QLD exhibits much higher success probability across most objective functions than other algorithms. Specifically, the phenomena of strong quantum tunneling and thermal effects equip QLD with superior capabilities to escape from local minima encircled by numerous shallow wells at the beginning of evolution. This advantage enables QLD to achieve nearly 100% success probability in the Michalewicz, Alpine 1, Bohachevsky 2, and Deflected Corrugated Spring (DCS) functions which own several not-so-deep wells. However, the persistence of quantum noise and thermal effects towards the end of the evolution process hinder QLD's ability to focus on the global minimum. Consequently, QLD performs poorly on the “Basin” function (Csendes), characterized by a flat region near the global minimum. The observations of dynamical processes in these experiments further confirms the three-phase explanation of QLD, which is shown at the end of Section VF.

Appendix B: Comparison of query complexity for different algorithms

In this appendix, we delve into the comparison of query complexity among various algorithms, i.e., the classical query complexity to local information and the quantum query complexity to the evaluation oracle [33, 76]. We assume that the quantum evaluation oracle O_V allows us to query the function value of V in a coherent way

$$O_V |x\rangle |z\rangle = |x\rangle |z + V(x)\rangle, \quad \forall x \in \mathbb{R}^d, z \in \mathbb{R}. \quad (\text{B1})$$

Correspondingly, there is a classical evaluation oracle O_V^l that allows us to query the function value of V in a local way. In the following, we will discuss the query complexity of QLD, QHD, QAA, SGD, and NAGD.

1. Quantum query complexity for QLD

The quantum query complexity associated with QLD can be inferred from the complexity involved in the simulation of the Lindblad system, given that QLD is a Lindblad system itself. Here, we mainly follow Proposition 4 to simulate QLD. Definition 1, Definition 2 and Proposition 3 are stated for the references in constructing block-encoded matrices used in Proposition 4.

Theorem 3. *Given a Lindblad equation with form Eq. (15),*

$$O\left((t(n^2 + \|V\|_{\max}) \frac{\log(t(n^2 + \|V\|_{\max})/\epsilon)}{\log \log(t(n^2 + \|V\|_{\max})/\epsilon)})\right)$$

queries to O_V are needed to simulate Eq. (15) for time t with error at most ϵ in terms of the diamond norm, where n is the number of discretization grids along each axis of domain and $\|V\|_{\max}$ is the max-norm of V .

Proof. We can divide Hamiltonian into two parts $H = E_k + V$. Then by finite difference method mentioned in Section IV B, it is very easy to present E_k and V in the matrix forms. Consider discretizing the domain into n grids along each axis, $E_k = -\frac{\hbar^2 \mathbf{L}}{2m\Delta x^2}$, where \mathbf{L} is the Laplacian matrix associated to the central difference method and Δx is the width of discretizing grid [33], and $V = \text{diag}(V(x_1), \dots, V(x_n))$ is a diagonal matrix by discretizing $V(x)$ in the grid, which is given by the oracle O_V [32].

By Definition 1, it is not difficult to give an $(\alpha_{E_k}, a, \xi_{E_k})$ -block-encoded matrix U_{E_k} of E_k and an (α_V, a, ξ_V) -block-encoded matrix U_V of V , where α_{E_k} is $O(\frac{1}{\Delta x^2}) = O(n^2)$ and α_V is $O(\|V\|_{\max})$. Then, Proposition 3 derives a $(\beta, a + b, \xi_{E_k} + \xi_V)$ -block-encoded matrix \tilde{W}_H of H with $\beta \geq |\alpha_{E_k}| + |\alpha_V|$. In addition, Proposition 3 also tells one query to \tilde{W}_H can be implemented by one query to U_{E_k} and one query to U_V .

Now, we have gotten a $(\beta, a + b, \xi_{E_k} + \xi_V)$ -block-encoded matrix \tilde{W}_H of H . In our Lindblad equation

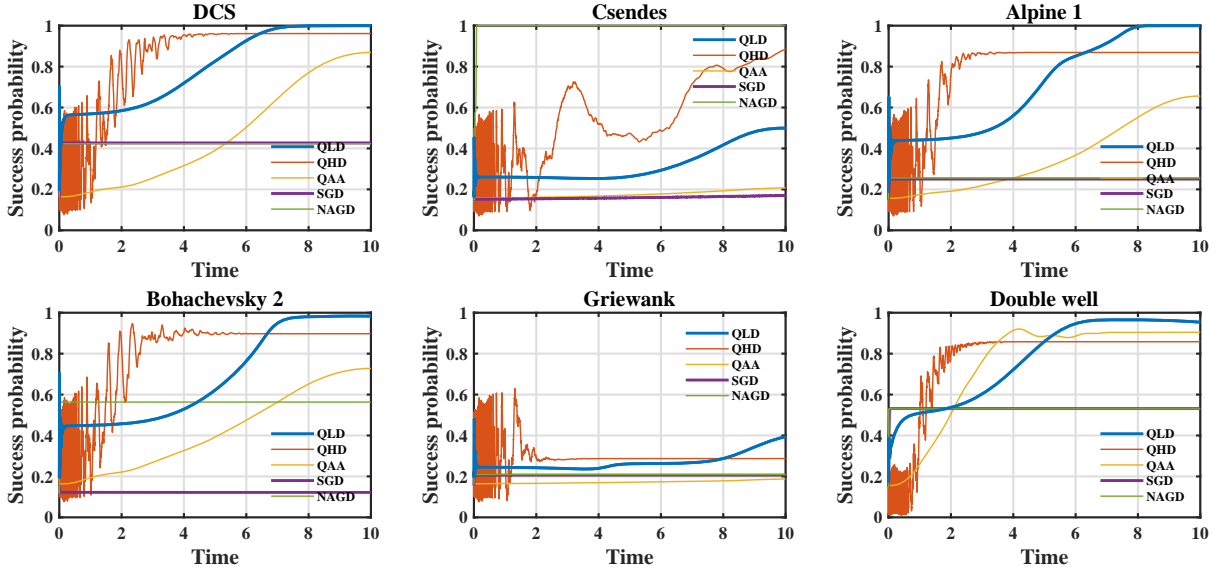


FIG. 20. Success probabilities of six objective functions for different algorithms at different (effective) evolution times.

Eq. (15), the unique L is given by $L = \mu x + i\nu p$. Presenting L in the matrix form by finite difference method, we have $L = \mu \cdot \text{diag}(x_1, \dots, x_n) + \nu \hbar \cdot \frac{\mathbf{D}}{\Delta x}$, where \mathbf{D} is the differential matrix associated to the central difference method. Then, we can easily give an (α_L, a, ξ_L) -block-encoded matrix U_L of L , where α_L is at most $O(\frac{1}{\Delta x}) = O(n)$.

Using Proposition 4, $\|\mathcal{L}\|_{\text{be}} = \beta + \alpha_L^2$, the smallest β we can achieve is $|\alpha_{E_k}| + |\alpha_V| = O(n^2) + O(\|V\|_{\text{max}})$, which gives $\|\mathcal{L}\|_{\text{be}} = O(n^2 + \|V\|_{\text{max}})$. So, $O\left(t(n^2 + \|V\|_{\text{max}}) \frac{\log(t(n^2 + \|V\|_{\text{max}})/\epsilon)}{\log \log(t(n^2 + \|V\|_{\text{max}})/\epsilon)}\right)$ queries to \tilde{W}_H and U_L are needed to simulate $e^{\mathcal{L}t}$ with error at most ϵ . Recall that each query to \tilde{W}_H can be implemented by one query to U_{E_k} and one query to U_V , and one query to U_V can be applied by one query to oracle O_V . So, $O\left(t(n^2 + \|V\|_{\text{max}}) \frac{\log(t(n^2 + \|V\|_{\text{max}})/\epsilon)}{\log \log(t(n^2 + \|V\|_{\text{max}})/\epsilon)}\right)$ queries to O_V are needed to simulate $e^{\mathcal{L}t}$ with error at most ϵ . \square

Definition 1 (Block-encoding, Definition 43 of Ref. [77]). Let $A \in \mathbb{C}^{2^q \times 2^q}$ be a q -qubit operator. Then a $(q+a)$ -qubit unitary U_A is an (α, a, ξ) block-encoding of A if

$$\|\alpha(|0^a\rangle \otimes I_q)U(|0^a\rangle \otimes I_q) - A\| \leq \xi.$$

Definition 2 (State preparation pair, Definition 51 of Ref. [77]). Let $y = (y_0, \dots, y_{m-1}) \in \mathbb{C}^m$ and $\|y\|_1 \leq \beta$. The pair of unitaries (P_L, P_R) is called a (β, q, ξ) -state-preparation pair for a nonzero vector y if $P_L|0^q\rangle = \sum_{j=0}^{2^q-1} c_j|j\rangle$ and $P_R|0^q\rangle = \sum_{j=0}^{2^q-1} d_j|j\rangle$ such that $\sum_{j=0}^{m-1} \beta(c_j^* d_j - y_j) \leq \xi$ and for all $j = m, m+1, \dots, 2^q-1$ we have $c_j^* d_j = 0$.

Proposition 3 (Linear combination of block-encoded matrices, Proposition 5 of Ref. [78]). Let $A =$

$\sum_{j=0}^{m-1} y_j A^{(j)}$ be a q -qubit operator, where $A^{(j)} \in \mathbb{C}^{2^q \times 2^q}$ and $y = (y_0, \dots, y_{m-1}) \in \mathbb{C}^m$. If U_j is an (α_j, a_j, ξ_j) -block-encoding of $A^{(j)}$ and (P_R, P_L) is a $(\beta, b, 0)$ -state-preparation pair for $(y_0 \alpha_0, y_1 \alpha_1, \dots, y_{m-1} \alpha_{m-1})$, then

$$\begin{aligned} \tilde{W}_A = & (P_L^\dagger \otimes I_{a+q}) \left(\sum_{j=0}^{m-1} |j\rangle \langle j| \otimes (I_{a-a_j} \otimes U_j) \right. \\ & \left. + \sum_{j=m}^{2^b-1} |j\rangle \langle j| \otimes I_{a+q} \right) (P_R \otimes I_{a+q}) \end{aligned}$$

is a $(\beta, a + b, \sum_{j=0}^{m-1} |y_j| \xi_j)$ -block-encoding of $A = \sum_{j=0}^{m-1} y_j A^{(j)}$, where $a = \max_j a_j$.

Proposition 4 (Complexity for Lindblad simulation, Theorem 11 of Ref. [79]). Suppose we are given an (α_0, a, ϵ') -block-encoding U_H of H and an (α_i, a, ϵ') -block-encoding U_{L_j} for each L_j ($j = 1, \dots, m$). For all $t, \epsilon \geq 0$ with $\epsilon' \leq \epsilon/(t\|\mathcal{L}\|_{\text{be}})$, there exists a quantum algorithm for simulating $e^{\mathcal{L}t}$ using

$$O\left(t\|\mathcal{L}\|_{\text{be}} \frac{\log(t\|\mathcal{L}\|_{\text{be}}/\epsilon)}{\log \log(t\|\mathcal{L}\|_{\text{be}}/\epsilon)}\right)$$

queries to U_H and U_{L_j} , and some additional 1- or 2-qubit gates, where $\|\mathcal{L}\|_{\text{be}} = \alpha_0 + \sum_{j=1}^m \alpha_j^2$.

2. Query complexity of other algorithms

a. Quantum query complexity for QHD

Because QHD simulates a time-dependent Hamiltonian system, its quantum query complexity can be inferred from the complexity involved in the simulation of the time-dependent Schrödinger equation. Here, we mainly follow Ref. [80, 81] and use quantum simulation in

the real space to calculate the quantum query complexity for QHD in terms of the quantum oracle O_V (Eq. (B1)).

Given a Nesterov's time-dependent $H(\tau) = \frac{2}{s_1 + \tau^3} (-\frac{1}{2}\nabla^2) + 2\tau^3 V(x)$ with $s_1 \ll 1$ [32], we can get the number of queries to O_V are $O\left(\|\tilde{V}\|_{\max,1} \frac{\log(\|\tilde{V}\|_{\max,1} t/\epsilon)}{\log \log(\|\tilde{V}\|_{\max,1} t/\epsilon)}\right)$ (by the Theorem 8 of Ref. [80], and the Theorem 4 and Lemma 9 of Ref. [81]), where $\tilde{V} = \tilde{V}(x, \tau) = 2\tau^3 V(x)$. Therefore, the total number of queries to O_V is

$$O\left((t^4 \|V\|_{\max}) \frac{\log((t^4 \|V\|_{\max})/\epsilon)}{\log \log((t^4 \|V\|_{\max})/\epsilon)}\right), \quad (\text{B2})$$

where the factor t^4 comes from the Nesterov's damping parameter τ^3 in $\tilde{V}(x, \tau)$.

b. Quantum query complexity for QAA

QAA is a quantum algorithm which evolves according to the time-dependent Schrödinger equation, so we mainly follow the Theorem 4 of Ref. [82] to calculate its query complexity. In the case of QAA, the total number of queries to O_V is

$$O\left(t \|V\|_{\max} \frac{\log(t \|V\|_{\max}/\epsilon)}{\log \log(t \|V\|_{\max}/\epsilon)}\right). \quad (\text{B3})$$

c. Classical query complexity for SGD

For SGD, we assume that the classical evaluation oracle O_V^{cl} allows us to query the function value of V in a

local way, so the total number of queries to O_V^{cl} is at least the number of iterations t/s timing the number of samples N_s , which derives $\Theta(N_s t/s)$ [33]. In the numerical experiment setting of Section V E 1, $s = \Delta t = O(\Delta x^2) = O(1/n^2)$, the query complexity becomes $\Theta(N_s t n^2)$.

d. Classical query complexity for NAGD

The classical query complexity for NAGD is same as SGD, which is $\Theta(N_s t/s)$. In the numerical experiment setting of Section V E 2, it becomes $\Theta(N_s t n^2)$.

3. Comparison of query complexity for different algorithms

From the above discussion, when t is significant, loosely speaking, QLD and QAA have similar quantum query complexity $\tilde{O}(t)$ which is much better than $\tilde{O}(t^4)$ of QHD. Furthermore, when the total evolution time is kept consistent across all quantum and classical algorithms, the quantum query complexity of QLD becomes comparable to those of SGD and NAGD, which are also $\tilde{O}(t)$.

This also indicates the superiority of QLD in scenario where the evolution time is significant.

-
- [1] J. Nocedal and S. J. Wright, *Numerical optimization* (Springer, 1999).
 - [2] Y. LeCun, Y. Bengio, and G. Hinton, Deep learning, *nature* **521**, 436 (2015).
 - [3] S. Ruder, An overview of gradient descent optimization algorithms, arXiv preprint arXiv:1609.04747 (2016).
 - [4] P. Jain, P. Kar, *et al.*, Non-convex optimization for machine learning, *Foundations and Trends in Machine Learning* **10**, 142 (2017).
 - [5] W. Su, S. Boyd, and E. Candes, A differential equation for modeling Nesterov's accelerated gradient method: theory and insights, *Advances in neural information processing systems* **27** (2014).
 - [6] A. Wibisono, A. C. Wilson, and M. I. Jordan, A variational perspective on accelerated methods in optimization, *proceedings of the National Academy of Sciences* **113**, E7351 (2016).
 - [7] M. I. Jordan, Dynamical, symplectic and stochastic perspectives on gradient-based optimization, in *Proceedings of the International Congress of Mathematicians: Rio de Janeiro 2018* (World Scientific, 2018) pp. 523–549.
 - [8] B. Shi, S. S. Du, M. I. Jordan, and W. J. Su, Understanding the acceleration phenomenon via high-resolution differential equations, *Mathematical Programming*, 1 (2021).
 - [9] B. Shi, W. J. Su, and M. I. Jordan, On learning rates and Schrödinger operators, arXiv preprint arXiv:2004.06977 (2020).
 - [10] M. Welling and Y. W. Teh, Bayesian learning via stochastic gradient Langevin dynamics, in *Proceedings of the 28th international conference on machine learning (ICML-11)* (2011) pp. 681–688.
 - [11] S. Ahn, A. Korattikara, and M. Welling, Bayesian posterior sampling via stochastic gradient Fisher scoring, arXiv preprint arXiv:1206.6380 (2012).
 - [12] T. Chen, E. Fox, and C. Guestrin, Stochastic gradient hamiltonian monte carlo, in *International conference on machine learning* (PMLR, 2014) pp. 1683–1691.
 - [13] Y. Zhang, P. Liang, and M. Charikar, A hitting time analysis of stochastic gradient Langevin dynamics, in *Conference on Learning Theory* (PMLR, 2017) pp. 1980–2022.
 - [14] R. Dwivedi, Y. Chen, M. J. Wainwright, and B. Yu, Log-concave sampling: Metropolis-Hastings algorithms are fast!, in *Conference on learning theory* (PMLR, 2018)

- pp. 793–797.
- [15] S. Chewi, Log-concave sampling, Book draft available at <https://chewiinho.github.io> (2022).
 - [16] T. Li, S. Chakrabarti, and X. Wu, Sublinear quantum algorithms for training linear and kernel-based classifiers, in *International Conference on Machine Learning* (PMLR, 2019) pp. 3815–3824.
 - [17] J. van Apeldoorn and A. Gilyén, Quantum algorithms for zero-sum games, arXiv preprint arXiv:1904.03180 (2019).
 - [18] P. A. Casares and M. A. Martin-Delgado, A quantum interior-point predictor–corrector algorithm for linear programming, *Journal of physics A: Mathematical and Theoretical* **53**, 445305 (2020).
 - [19] A. Bouland, Y. M. Getachew, Y. Jin, A. Sidford, and K. Tian, Quantum speedups for zero-sum games via improved dynamic Gibbs sampling, in *International Conference on Machine Learning* (PMLR, 2023) pp. 2932–2952.
 - [20] M. Gao, Z. Ji, T. Li, and Q. Wang, Logarithmic-Regret quantum learning algorithms for zero-sum games, arXiv preprint arXiv:2304.14197 (2023).
 - [21] F. G. Brandão and K. M. Svore, Quantum speed-ups for solving semidefinite programs, in *2017 IEEE 58th Annual Symposium on Foundations of Computer Science (FOCS)* (IEEE, 2017) pp. 415–426.
 - [22] J. van Apeldoorn, A. Gilyén, S. Gribling, and R. de Wolf, Quantum SDP-solvers: Better upper and lower bounds, in *2017 IEEE 58th Annual Symposium on Foundations of Computer Science (FOCS)* (IEEE, 2017) pp. 403–414.
 - [23] F. G. Brandão, A. Kalev, T. Li, C. Y.-Y. Lin, K. M. Svore, and X. Wu, Quantum SDP solvers: Large speedups, optimality, and applications to quantum learning, arXiv preprint arXiv:1710.02581 (2017).
 - [24] J. van Apeldoorn and A. Gilyén, Improvements in quantum SDP-solving with applications, in *46th International Colloquium on Automata, Languages, and Programming (ICALP 2019)* (Schloss Dagstuhl-Leibniz-Zentrum fuer Informatik, 2019).
 - [25] I. Kerenidis and A. Prakash, A quantum interior point method for LPs and SDPs, *ACM Transactions on Quantum Computing* **1**, 1 (2020).
 - [26] B. Augustino, G. Nannicini, T. Terlaky, and L. F. Zuluaga, Quantum interior point methods for semidefinite optimization, *Quantum* **7**, 1110 (2023).
 - [27] P. Rebentrost, M. Schuld, L. Wossnig, F. Petruccione, and S. Lloyd, Quantum gradient descent and Newton’s method for constrained polynomial optimization, *New Journal of Physics* **21**, 073023 (2019).
 - [28] K. Li, S. Wei, P. Gao, F. Zhang, Z. Zhou, T. Xin, X. Wang, P. Rebentrost, and G. Long, Optimizing a polynomial function on a quantum processor, *npj Quantum Information* **7**, 16 (2021).
 - [29] S. Chakrabarti, A. M. Childs, T. Li, and X. Wu, Quantum algorithms and lower bounds for convex optimization, *Quantum* **4**, 221 (2020).
 - [30] J. van Apeldoorn, A. Gilyén, S. Gribling, and R. de Wolf, Convex optimization using quantum oracles, *Quantum* **4**, 220 (2020).
 - [31] C. Zhang, J. Leng, and T. Li, Quantum algorithms for escaping from saddle points, *Quantum* **5**, 529 (2021).
 - [32] J. Leng, E. Hickman, J. Li, and X. Wu, Quantum Hamiltonian descent, arXiv preprint arXiv:2303.01471 (2023).
 - [33] Y. Liu, W. J. Su, and T. Li, On quantum speedups for nonconvex optimization via quantum tunneling walks, *Quantum* **7**, 1030 (2023).
 - [34] D. S. Ray, Notes on Brownian motion and related phenomena, arXiv preprint physics/9903033 (1999).
 - [35] C. W. Gardiner *et al.*, *Handbook of stochastic methods*, Vol. 3 (Springer Berlin, 1985).
 - [36] C. Gardiner and P. Zoller, *Quantum noise: a handbook of Markovian and non-Markovian quantum stochastic methods with applications to quantum optics* (Springer Science & Business Media, 2004).
 - [37] G. Ford, M. Kac, and P. Mazur, Statistical mechanics of assemblies of coupled oscillators, *Journal of Mathematical Physics* **6**, 504 (1965).
 - [38] J. J. Sakurai and E. D. Commins, *Modern quantum mechanics*, revised edition (1995).
 - [39] A. Lampo, M. Á. G. March, and M. Lewenstein, *Quantum Brownian motion revisited: extensions and applications* (Springer, 2019).
 - [40] A. O. Caldeira and A. J. Leggett, Path integral approach to quantum Brownian motion, *Physica A: Statistical mechanics and its Applications* **121**, 587 (1983).
 - [41] S. Gao, Dissipative quantum dynamics with a Lindblad functional, *Physical review letters* **79**, 3101 (1997).
 - [42] L. Diósi, On high-temperature Markovian equation for quantum Brownian motion, *Europhysics Letters* **22**, 1 (1993).
 - [43] R. Karrlein and H. Grabert, Exact time evolution and master equations for the damped harmonic oscillator, *Physical Review E* **55**, 153 (1997).
 - [44] B. Shi, On the hyperparameters in stochastic gradient descent with momentum, arXiv preprint arXiv:2108.03947 (2021).
 - [45] G. Ford and M. Kac, On the quantum Langevin equation, *Journal of statistical physics* **46**, 803 (1987).
 - [46] G. Lindblad, On the generators of quantum dynamical semigroups, *Communications in Mathematical Physics* **48**, 119 (1976).
 - [47] In multidimensional case, it should be $[x, p] = \sum_j e_j \otimes e^j i\hbar I$, for simplicity, we write it as $[x, p] = i\hbar$.
 - [48] H. Goldstein, C. Poole, and J. Safko, *Classical mechanics* (2002).
 - [49] A. Kudlis, I. Iorsh, and I. Tokatly, Dissipation and spontaneous emission in quantum electrodynamical density functional theory based on optimized effective potential: A proof of concept study, *Physical Review B* **105**, 054317 (2022).
 - [50] M. François, Symplectic Leap Frog Scheme (2023), <https://www.mathworks.com/matlabcentral/fileexchange/38652-symplectic-leap-frog-scheme>, Last accessed on 2023-9-15, MATLAB Central File Exchange.
 - [51] This parameter setting is also consistent with Refs. [41, 52, 75] after nondimensionalizing.
 - [52] S. Gao, Lindblad approach to quantum dynamics of open systems, *Physical Review B* **57**, 4509 (1998).
 - [53] A. O. Caldeira and A. J. Leggett, Quantum tunnelling in a dissipative system, *Annals of physics* **149**, 374 (1983).
 - [54] E. G. Harris, Quantum tunneling in dissipative systems, *Physical Review A* **48**, 995 (1993).
 - [55] S. Chakravarty and A. J. Leggett, Dynamics of the two-state system with ohmic dissipation, *Physical review letters* **52**, 5 (1984).
 - [56] A. J. Leggett, S. Chakravarty, A. T. Dorsey, M. P. Fisher, A. Garg, and W. Zwerger, Dynamics of the dissipa-

- tive two-state system, *Reviews of Modern Physics* **59**, 1 (1987).
- [57] M. P. Fisher and A. T. Dorsey, Dissipative quantum tunneling in a biased double-well system at finite temperatures, *Physical review letters* **54**, 1609 (1985).
 - [58] P. Hanggi, Escape from a metastable state, *Journal of Statistical Physics* **42**, 105 (1986).
 - [59] N. Kelkar, D. L. Gómez, and E. J. Patino, Time in dissipative tunneling: subtleties and applications, *Annals of Physics* **382**, 11 (2017).
 - [60] D. Dolgitzter, D. Zeng, and Y. Chen, Dynamical quantum phase transitions in the spin-boson model, *Optics Express* **29**, 23988 (2021).
 - [61] This integral does not have an analytical solution, and it is also non-integrable when the interval of integration includes 0. However, in the situations we are considering (such as numerical experiments), we can give T a finite lower bound, thus making this integral integrable.
 - [62] A. Layeb, New hard benchmark functions for global optimization, arXiv preprint arXiv:2202.04606 (2022).
 - [63] C. A. Floudas, P. M. Pardalos, C. Adjiman, W. R. Espósito, Z. H. Gümus, S. T. Harding, J. L. Klepeis, C. A. Meyer, and C. A. Schweiger, *Handbook of test problems in local and global optimization*, Vol. 33 (Springer Science & Business Media, 2013).
 - [64] A. R. Al-Roomi, Unconstrained single-objective benchmark functions repository, Dalhousie University, Electrical and Computer Engineering, Halifax, Nova Scotia, Canada (2015).
 - [65] M. Jamil and X.-S. Yang, A literature survey of benchmark functions for global optimisation problems, *International Journal of Mathematical Modelling and Numerical Optimisation* **4**, 150 (2013).
 - [66] S. Surjanovic and D. Bingham, Virtual library of simulation experiments: Test functions and datasets, Retrieved September 14, 2023, from <http://www.sfu.ca/~ssurjano> (2023).
 - [67] F. J. Richards, A flexible growth function for empirical use, *Journal of experimental Botany* **10**, 290 (1959).
 - [68] The original form of Ref. [32] set s_2 to zero, however, our symplectic leapfrog scheme is not as stable as shifted Fourier transform used in Ref. [32]. In order to maintain the stability of numerical calculation in symplectic leapfrog scheme, we also set s_2 to be a small positive number.
 - [69] E. Farhi, J. Goldstone, S. Gutmann, J. Lapan, A. Lundgren, and D. Preda, A quantum adiabatic evolution algorithm applied to random instances of an NP-complete problem, *Science* **292**, 472 (2001).
 - [70] D. J. Griffiths and D. F. Schroeter, *Introduction to quantum mechanics* (Cambridge university press, 2018).
 - [71] J. Cohen, A. Khan, and C. Alexander, Portfolio optimization of 60 stocks using classical and quantum algorithms, arXiv preprint arXiv:2008.08669 (2020).
 - [72] P. Date and T. Potok, Adiabatic quantum linear regression, *Scientific reports* **11**, 21905 (2021).
 - [73] Y. E. Nesterov, A method of solving a convex programming problem with convergence rate $O(1/k^2)$, in *Doklady Akademii Nauk*, Vol. 269 (Russian Academy of Sciences, 1983) pp. 543–547.
 - [74] W. H. Press, *Numerical recipes 3rd edition: The art of scientific computing* (Cambridge university press, 2007).
 - [75] S. Gao, D. Busch, and W. Ho, Femtosecond dynamics of electron-vibrational heating and desorption, *Surface science* **344**, L1252 (1995).
 - [76] A. M. Childs, T. Li, J.-P. Liu, C. Wang, and R. Zhang, Quantum algorithms for sampling log-concave distributions and estimating normalizing constants, *Advances in Neural Information Processing Systems* **35**, 23205 (2022).
 - [77] A. Gilyén, Y. Su, G. H. Low, and N. Wiebe, Quantum singular value transformation and beyond: exponential improvements for quantum matrix arithmetics, in *Proceedings of the 51st Annual ACM SIGACT Symposium on Theory of Computing* (2019) pp. 193–204.
 - [78] S. Takahira, A. Ohashi, T. Sogabe, and T. S. Usuda, Quantum algorithms based on the block-encoding framework for matrix functions by contour integrals, arXiv preprint arXiv:2106.08076 (2021).
 - [79] X. Li and C. Wang, Simulating Markovian open quantum systems using higher-order series expansion, arXiv preprint arXiv:2212.02051 (2022).
 - [80] A. M. Childs, J. Leng, T. Li, J.-P. Liu, and C. Zhang, Quantum simulation of real-space dynamics, *Quantum* **6**, 860 (2022).
 - [81] J. Leng, Y. Zheng, and X. Wu, A quantum-classical performance separation in nonconvex optimization, arXiv preprint arXiv:2311.00811 (2023).
 - [82] D. W. Berry, A. M. Childs, Y. Su, X. Wang, and N. Wiebe, Time-dependent Hamiltonian simulation with L^1 -norm scaling, *Quantum* **4**, 254 (2020).

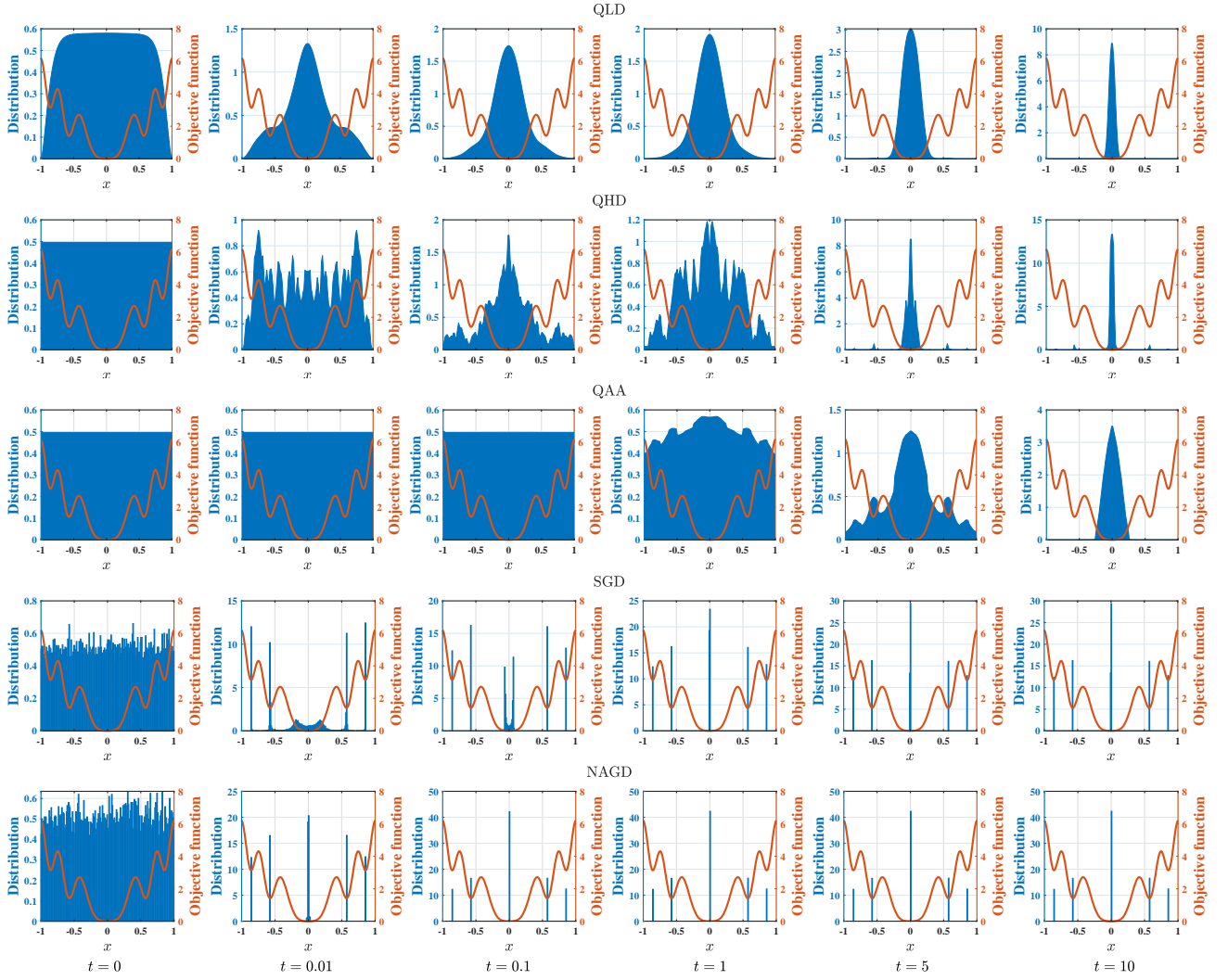
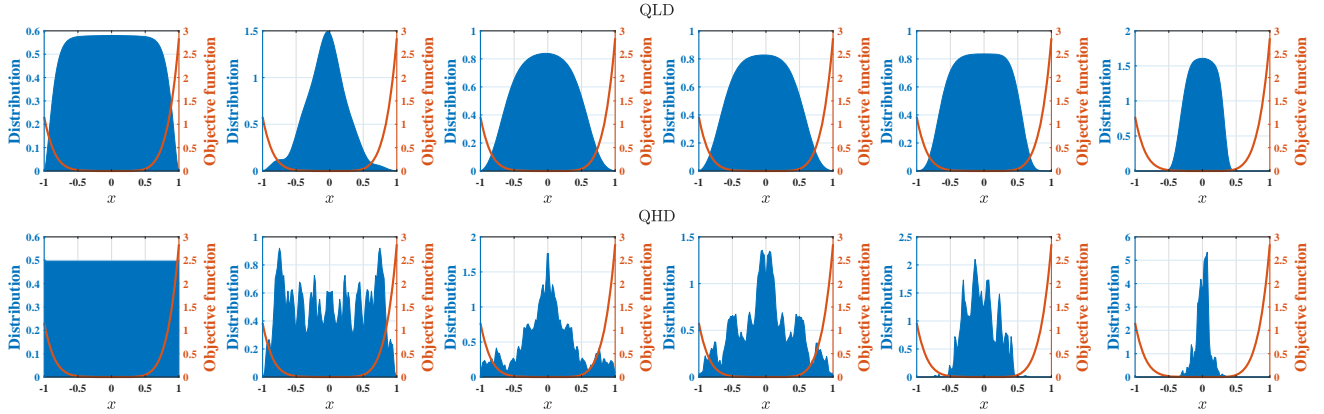


FIG. 21. Probability distributions of DCS function ($x^* = 0$) for different algorithms at different (effective) evolution times $t = 0, 0.01, 0.1, 1, 5, 10$.



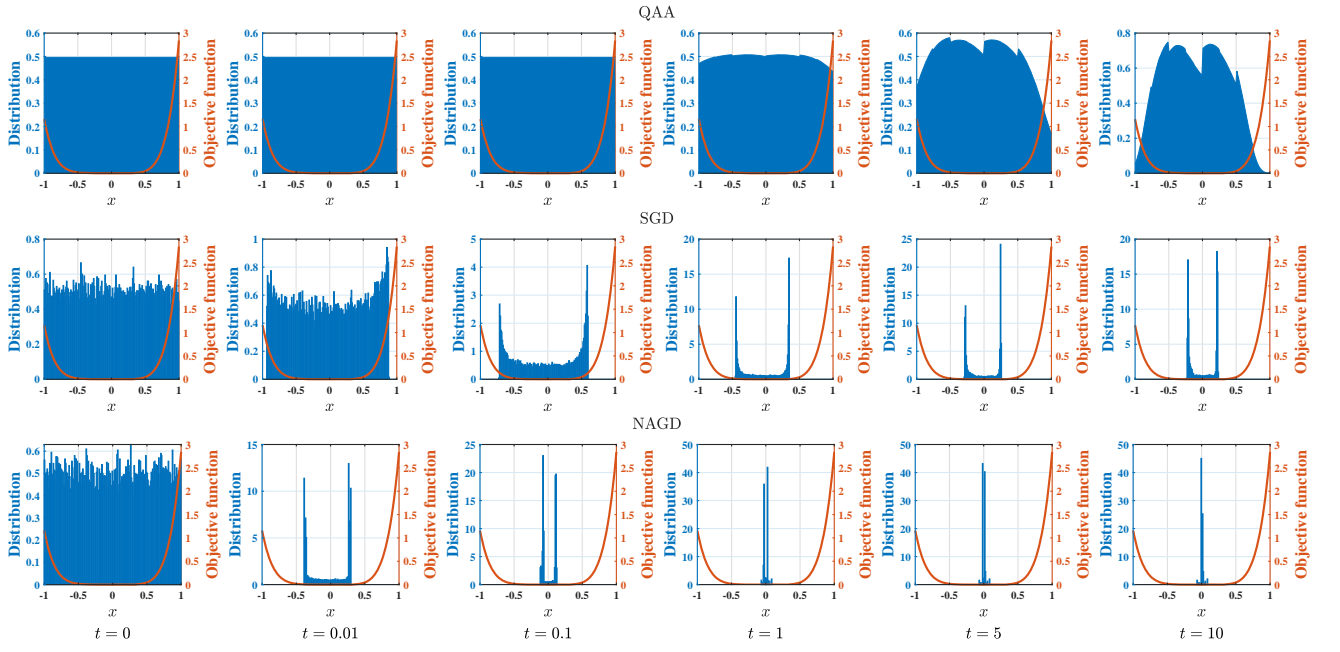
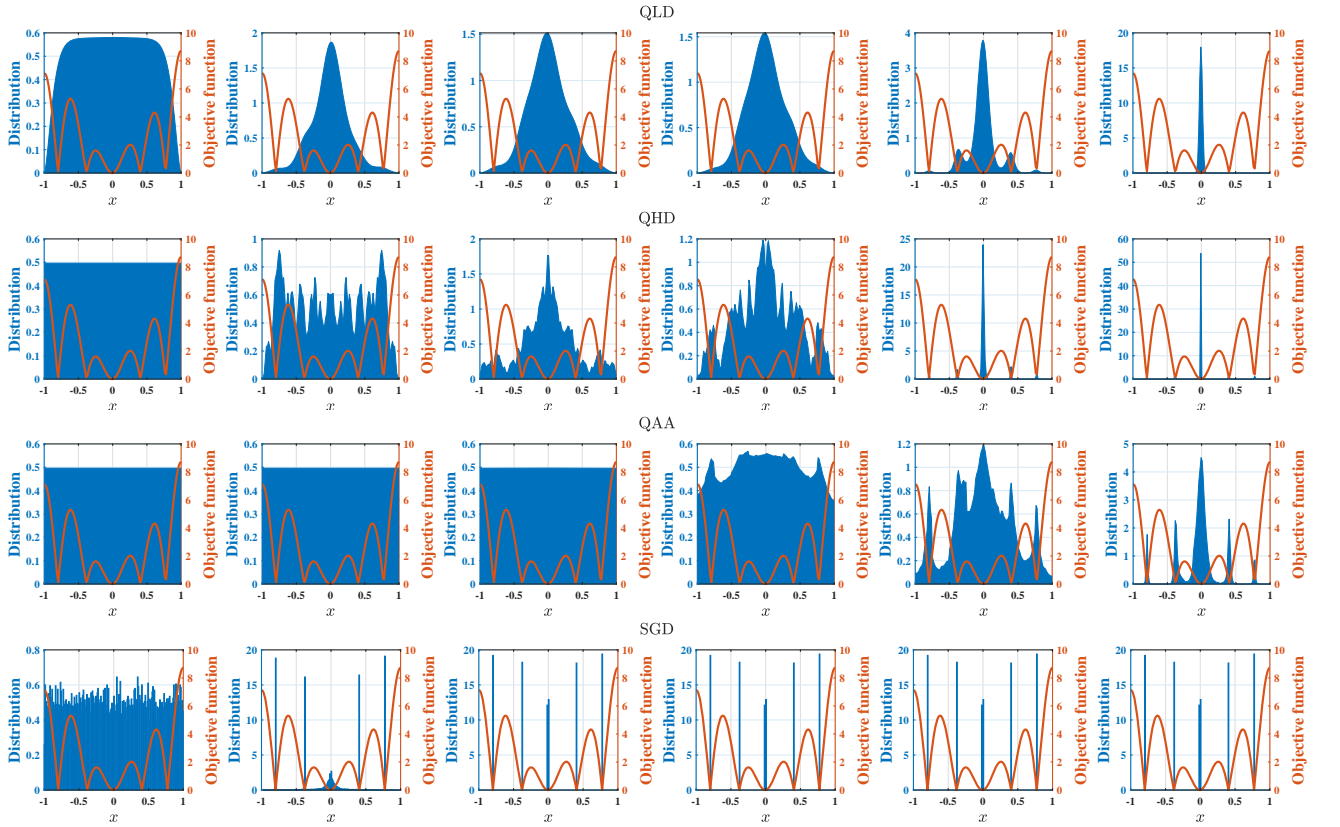


FIG. 22. Probability distributions of Csendes function ($x^* = 0$) for different algorithms at different (effective) evolution times $t = 0, 0.01, 0.1, 1, 5, 10$.



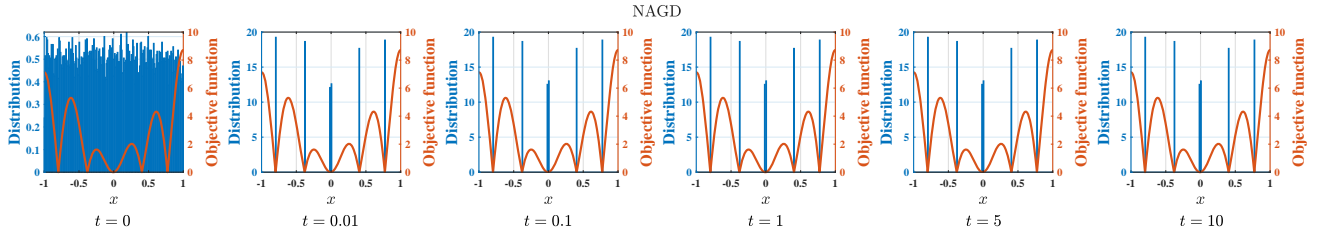


FIG. 23. Probability distributions of Alpine 1 function ($x^* = 0$) for different algorithms at different (effective) evolution times $t = 0, 0.01, 0.1, 1, 5, 10$.

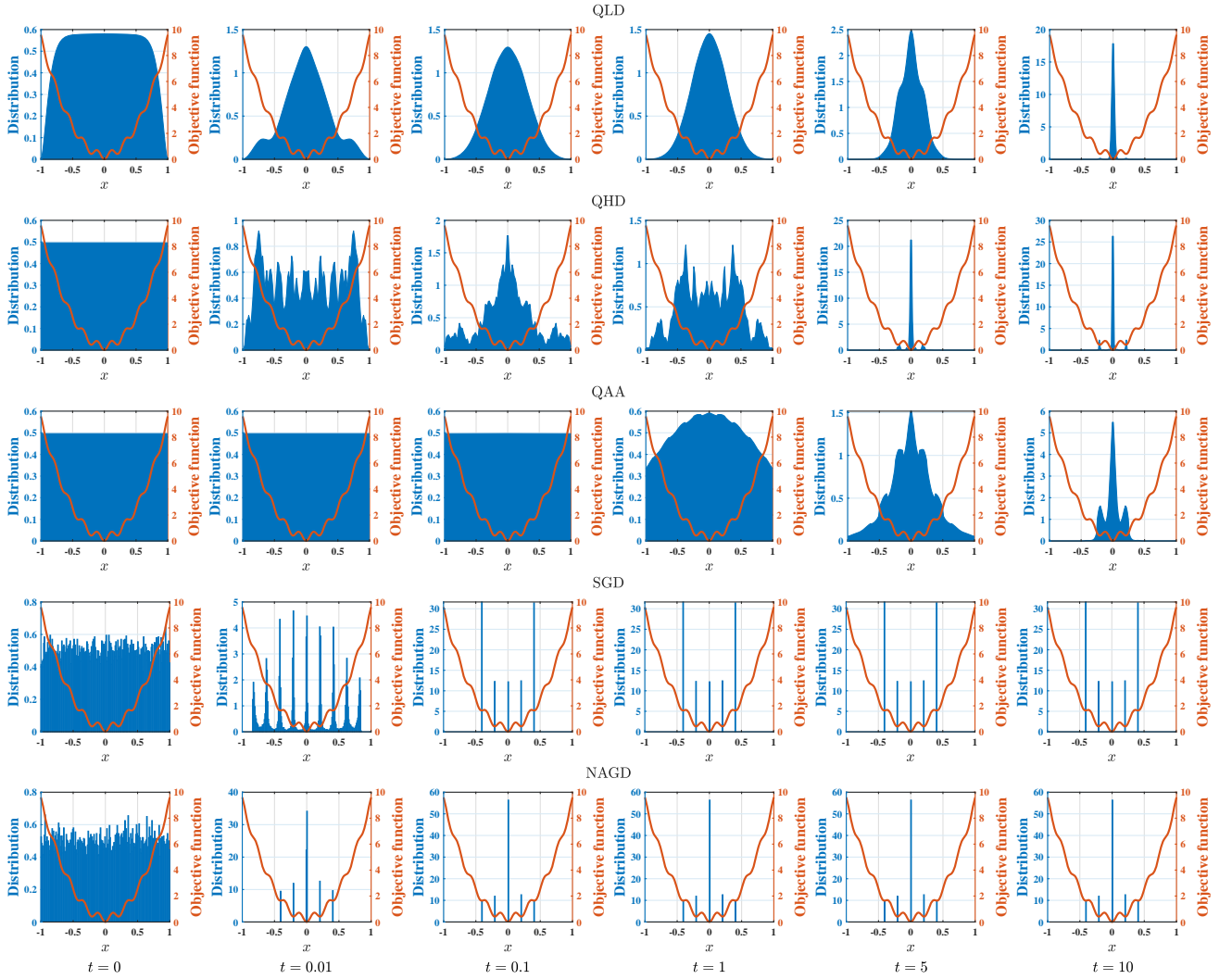


FIG. 24. Probability distributions of Bohachevsky 2 function ($x^* = 0$) for different algorithms at different (effective) evolution times $t = 0, 0.01, 0.1, 1, 5, 10$.

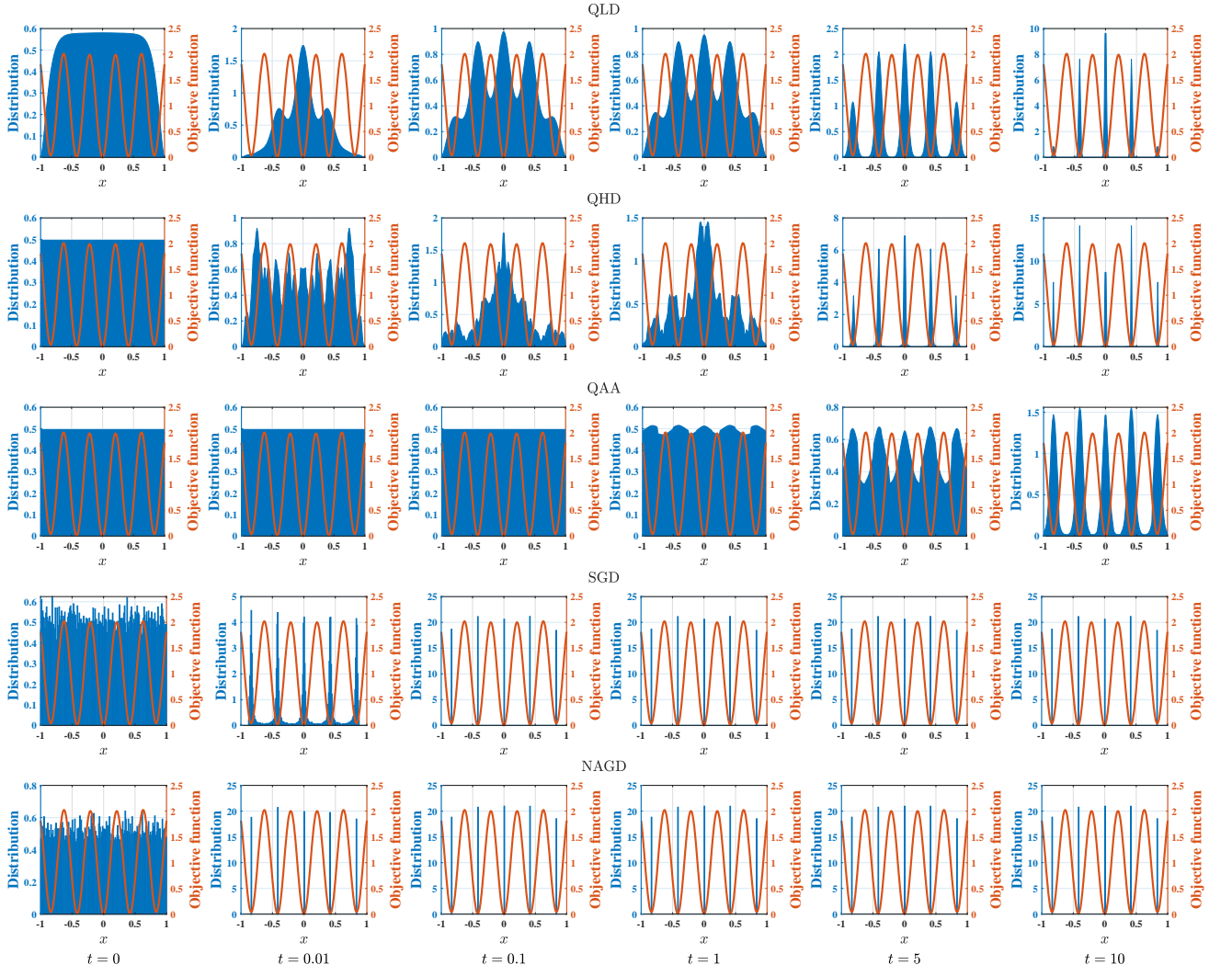
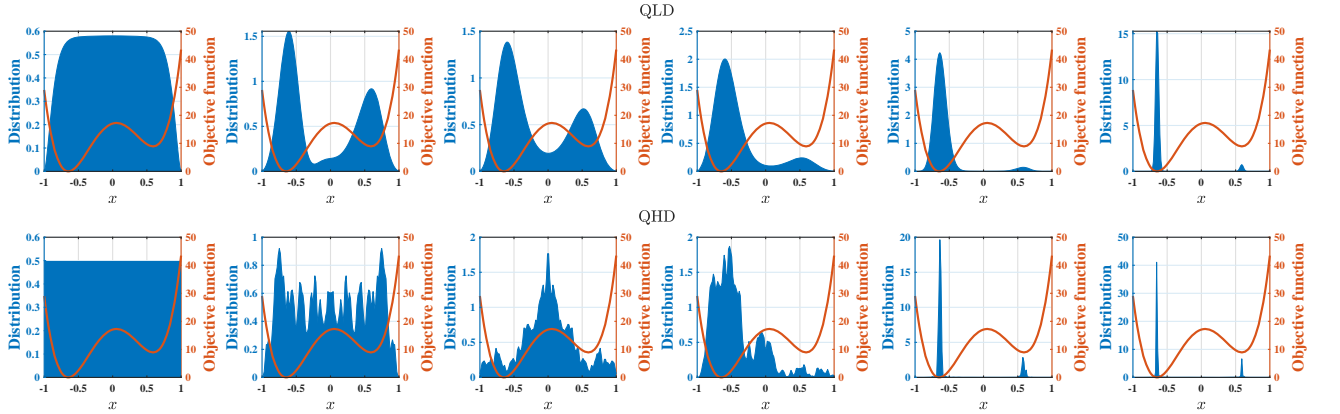


FIG. 25. Probability distributions of Griewank function ($x^* = 0$) for different algorithms at different (effective) evolution times $t = 0, 0.01, 0.1, 1, 5, 10$.



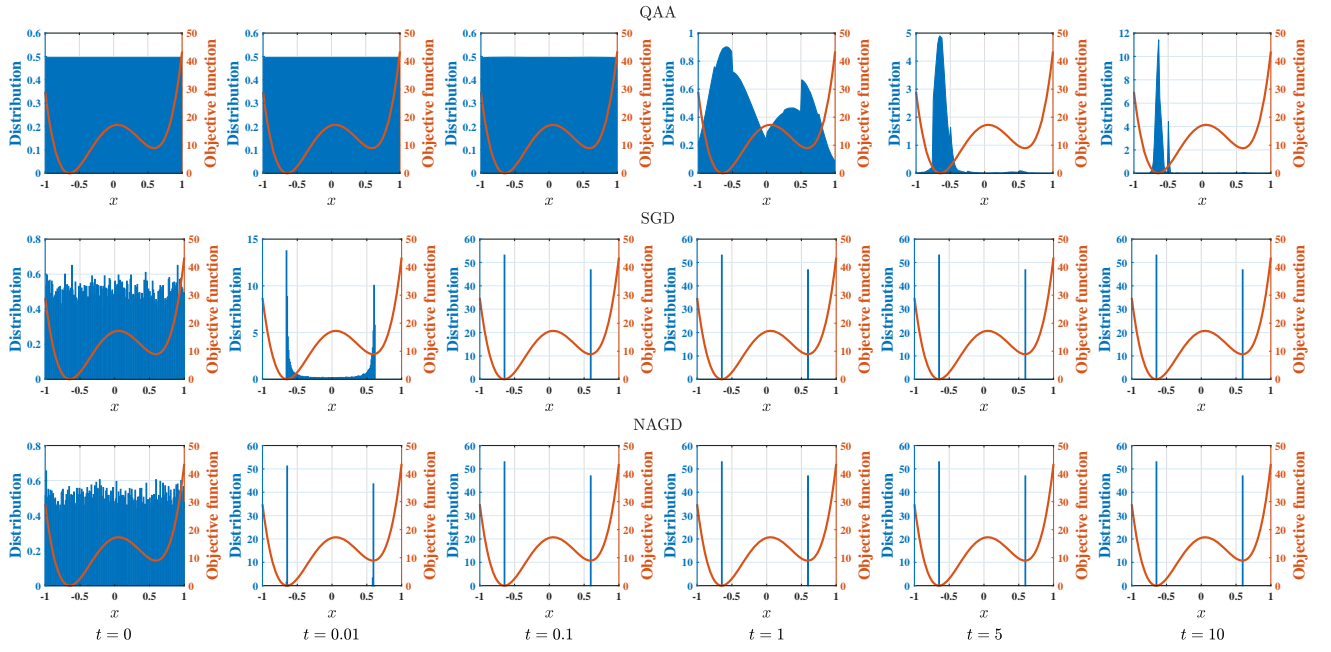


FIG. 26. Probability distributions of Double well function ($x^* = -0.6472$) for different algorithms at different (effective) evolution times $t = 0, 0.01, 0.1, 1, 5, 10$.